Master Thesis
Computational Mechanics

Computational study of the spatio-temporal response of oscillatory electrochemical systems in arrangements of one and two electrode pairs

Panagiotis Stamatopoulos
Stud.Code: 52113029
Supervisor: Assistant Prof. Karantonis Antonis

October, 2015

National Tachnical University of Athens
School of Chemical Engineering

Contents

Acknowledgements

I would like to thank most sincerely Prof. Antonis Karantonis, for his enthusiastic support and guidance from the time of my initial proposal. He made my thesis work far more enjoyable than would otherwise have been the case. I am most grateful to have benefited from the supervision of such distinguished academic and acknowledged scientist in the field.

Abstract

The aim of the present work is the computational study of the spatial and temporal response of electrochemical systems where oscillations are observed (electrochemical oscillators). The developed models were studied numerically with the method of finite elements, by taking into account systems of two electrodes (anode and cathode), functioning under constant potential conditions. These systems were studied by assuming tertiary current distribution and the spatio-temporal variations of the potential and concentrations in the solution were determined. The effect of the applied potential and the geometry on the non-linear response was studied also. Finally, a computational study was performed for simple networks of electrochemical oscillators, consisting of two oscillatory electrode pairs and the type of coupling was investigated.

Σκοπός της παρούσας εργασίας είναι η υπολογιστική μελέτη της χωρικής και χρονικής απόκρισης ηλεκτροχημικών συστημάτων που έχουν τη δυνατότητα να ταλαντώνονται στο χρόνο (ηλεκτροχημικοί ταλαντωτές). Για το λόγο αυτό, αναπτύχθηκαν μοντέλα τα οποία επιλύθηκαν υπολογιστικά με τη μέθοδο των πεπερασμένων στοιχείων, που περιγράφουν ηλεκτροχημικές διατάξεις δύο ηλεκτροδίων (άνοδος και κάθοδος) οι οποίες λειτουργούν υπό συνθήκες σταθερά επιβαλλόμενου ηλεκτρικού δυναμικού. Μελετήθηκε η ταλαντούμενη απόκριση τέτοιων συστημάτων, θεωρώντας τριτογενή κατανομή ηλεκτρικού ρεύματος, και υπολογίσθηκαν οι χωρο-χρονικές μεταβολές του ηλεκτρικού δυναμικού και των συγκεντρώσεων στο ηλεκτρολυτικό διάλυμα. Διερευνήθηκε η επίδραση του εφαρμοζόμενο δυναμικού και της γεωμετρίας στη μη-γραμμική δυναμική απόκριση. Τέλος, μελετήθηκαν υπολογιστικά, απλά δίκτυα ηλεκτροχημικών ταλαντωτών αποτελούμενα από δύο ζεύγη ηλεκτροδίων και διερευνήθηκε το είδος της σύζευξής τους.

Nomenclature

$\mathbf{v}$	fluid velocity vector (m/s)
$\mathbf{N_i}$	mass flux of ionic species i (mol/(m^2·s))
η_i	overpotential of each electrode (V)
$\nu_{i,m}$	stoichiometric coefficient
Φ_i	electric potential (V)
Φ_ℓ	electric potential in solution (V)
$\Phi_{\mathrm{ext_a}}$	applied electrode voltage (V)
σ	conductivity (S/cm)
c_i	concentrations of ionic species i (mol/m^3)
C_{dl}	electrical double layer capacitance (F/m^2)
D_i	diffusion coefficient of ionic species i (10^{-9}m^2·s)
F	Faraday constant (C/mol)
i	number of species, index
$i_{\mathrm{F_a}}$	Faradaic current density on anode (A)
i_{loc}	charge transfer current density (A/m^2)
k_i	potential dependent reaction rate coefficient
k_i^*	temperature dependent reaction rate coefficient
m	number of reaction, index
R	universal gas constant (8.3143 j/ mole· K)
T	Thermodynamic absolute temperature (293.15 K)
u_i	ionic mobility of a species i (s·mol/kg)
z_i	number of electric charge of ionic species i

Chapter 1

Introduction

Many electrochemical systems exhibit instabilities leading to oscillations of the current, under potentiostatic conditions [3]. The oscillations observed experimentally are usually of periodic type and its characteristics (amplitude and period) are determined by the kinetics of electrochemical reactions taking place on the electrodes, the mass transport phenomena in the electrolytic solution and the geometric characteristics of the electrolytic cell.

The determination of the kinetics of such oscillating systems are extremely difficult, due to the complexity of the mechanism. Moreover, the quantitative modeling of such systems is limited due to the unknown values of the kinetic constants. Even when the kinetics are known or accepted, the resulting equations are difficult to solve [17]. The resulting mathematical problem is a system of partial differential equations (PDEs) with non-linear boundary conditions (the kinetic equations on the electrode surfaces). Therefore, the modeling of these non-linear dynamical systems is usually restricted due to necessary assumptions. The most common assumption is to use the model of the Nernst diffusion layer where it is considered that all changes of the concentrations of chemical species occurs within a restricted, fixed-length layer, near the electrodes, and that the concentration distributions are linear within the fixed layer. Beyond this layer, all concentrations are assumed constant. This approach converts the PDE problem to an ordinary differential equations problem (ODE) [10]. Remarkably, this option is able to describe qualitatively the instabilities and oscillations but it cannot give realistic results on the phenomena occurring in the electrolytic solution. Moreover, this approach cannot predict changes due to the modification of geometry of the electrolytic cell. Another approach ignores changes in the electrolytic solution and is able to model exclusively surface phenomena, i.e. concentrations and potential distributions on the electrode surface [4].

In this study, the modelling of electrochemical oscillatory systems is based on an approach considering only few assumptions and eliminating the need of the Nernst diffusion layer model. Typical two electrode arrangements (anode and cathode) are considered, in the absence of a reference electrode. It is as-

sumed that the description of the flow of the chemical species is determined by the Nernst-Planck equation, taking into account both the diffusion and the electromigration of the particles under the influence of the electric field. Moreover, the kinetics on the electrodes are taken into account. Thus, in terms of current distribution, a tertiary current distribution model is considered. In order to maintain the generality of the approach, a specific mechanism of electrochemical reactions is not considered, but a general non-linear dependence of faradaic current from the electrode potential is introduced. The formalism is implemented for both one and two dimensions and summarizes the impact of kinetic and geometrical characteristics in the appearance of oscillations under potentiostatic conditions. Additionally, simple networks of electrochemical oscillators are studied numerically in order to elucidate the interaction mechanism of such non linear oscillators [9, 6, 7, 13, 16].

Chapter 2

Physical Model and Mathematical Formulation

2.1 Physical Model

The mathematical formulation depends on the reaction kinetics on the electrode(s) surface. Let us consider an anode where a dissolution / passivation reaction takes place. This reaction is, in principle, a multi-step electrode reaction including both parallel and consecutive steps. These may include the active dissolution of the metal, the formation of adsorbed species, the precipitation of salts and the formation of oxide (passive) layers. In the most simple case, the following scenario can be considered,

$$\mathrm{M} \xrightarrow{k_1} \mathrm{M}^{2+} + 2\mathrm{e} \tag{2.1}$$

$$\mathrm{M} + \mathrm{A} \underset{k_{-2}}{\overset{k_2}{\rightleftharpoons}} \mathrm{MA}^{2+}_{\mathrm{ads}} + 2\mathrm{e} \tag{2.2}$$

where M is the solid metal, M^{2+} the metal ions, A the solution species and MA^{2+} the adsorbed species "passivating" the metal surface.

The kinetic constants for the above simple scheme are potential dependent,

$$k_1 = k_1^* e^{\frac{2a_1F}{RT}E} \tag{2.3}$$

$$k_2 = k_2^* e^{\frac{2a_2F}{RT}E} \tag{2.4}$$

$$k_{-2} = k_{-2}^* e^{\frac{-2a_{-2}F}{RT}E} \tag{2.5}$$

where E is the electrode potential, a_i the symmetry factor and k_i^* the temperature dependent kinetic constants (the rest of the symbols have their usual meaning).

The total faradaic current due to the above reactions is,

$$i_{\mathrm{F}} = 2FS_{\max}[(k_1 + k_2 c_{\mathrm{A}})(1-\theta) - k_{-2}\theta] \tag{2.6}$$

where c_{A} the concentration of species A on the electrode surface, $S_{\max}$ is the surface concentration of adsorbed species at maximum coverage and $\theta = c_{\mathrm{MA}^{2+}_{\mathrm{ads}}}/S_{\max}$ the coverage.

The mass balance equation for the coverage is,

$$\frac{d\theta}{dt} = k_2 c_{\mathrm{A}}(1-\theta) - k_{-2}\theta \tag{2.7}$$

Assuming steady-state for the coverage we arrive to the following equation,

$$\theta = \frac{k_2 c_{\mathrm{A}}}{k_2 c_{\mathrm{A}} + k_{-2}} \tag{2.8}$$

thus, equation (2.6) is written,

$$i_{\mathrm{F}} = 2FS_{\max}\frac{k_1 k_{-2}}{k_2 c_{\mathrm{A}} + k_{-2}} \tag{2.9}$$

where its has to be noticed that all kinetic constants are potential dependent.

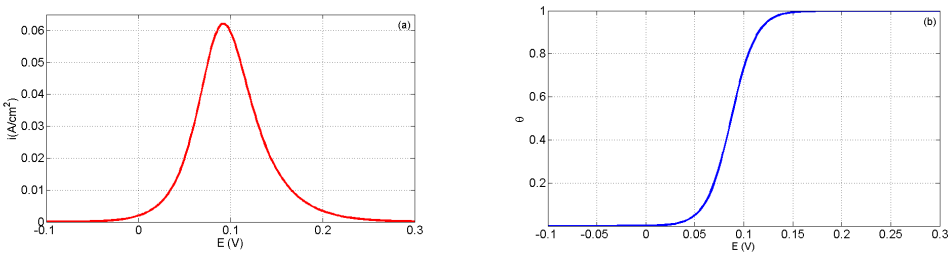

Figure 2.1: (a) Characteristic $i-E$ curve for dissolution-passivation mechanism and (b) corresponding change of the coverage.

A characteristic $i-E$ curve and the corresponding change of coverage for the above physical model is shown in Figure (2.1). It is evident that for small values of the potential, the current increases due to the electrodissolution of the metal. As the potential is increased, the current attains a maximum and then decreases due to passivation. It is known that this type of relation is observed in many electrochemical systems manifesting oscillations under potentiostatic conditions [12].

If double layer effects are to be taken into account, the Helmholtz model can be implemented. Thus, a charging current is considered at the anode,

$$i_{\mathrm{C}} = C_{\mathrm{dl}}\frac{dE}{dt} \tag{2.10}$$

where $C_{\rm dl}$ is the specific capacitance of the anode. Thus, the total current density at the anode is, $i = i_{\rm F} + i_{\rm c}$.

Concerning the cathode, a typical arrangement may incorporate an electrode where a (quasi)reversible reaction takes place,

$$\mathrm{N}^{2+} + 2\mathrm{e} \underset{k_{-3}}{\overset{k_3}{\rightleftharpoons}} \mathrm{N} \tag{2.11}$$

for example, the deposition/dissolution of a copper wire. In this case, the current-potential relation at the cathode attains the following equation,

$$i'_{\rm F} = i_0[e^{\frac{2a_3F}{RT}(E'-E_{\rm eq})} - \frac{c_{\mathrm{N}^{2+}}}{c^*_{\mathrm{N}^{2+}}} e^{\frac{2a_3F}{RT}(E'-E_{\rm eq})}] \tag{2.12}$$

where i_0 is the exchange current density of the reaction, $c^*_{\mathrm{N}^{2+}}$ is the bulk concentration of the cations of the metal N, E' the potential of the cathode and $E_{\rm eq}$ the equilibrium potential of $\mathrm{N}^{2+}|\mathrm{N}$. Double layer effects can be also introduced as shown above. Thus, the total current density at the cathode, i' will be the sum of the faradaic and charging current on this electrode. Apparently, during operation of the electrochemical cell,

$$I = I' = Ai = A'i' \tag{2.13}$$

where A and A' are the surface area of the anode and cathode, respectively.

2.2 Mathematical Formulation

In this section, several examples of electrochemical modeling, based on the secondary current distribution will be presented, as well as some simple analytic solutions.

Additionally, the ODE formulation of the problem is introduced. As mentioned in the introduction §1, several assumptions have to be considered. Despite the fact that the ODE formulation is able to reproduce the instabilities and the oscillations, an amount of physical information is lost.

Moreover, a more realistic PDE formulation is presented, based on tertiary current distribution. The tertiary current distribution accounts for electromigration effects, effects of electrodes kinetics and the effect of concentration variation in the cell.

2.2.1 Secondary current distribution

Let us consider an electrochemical cell consisting of two electrodes (1) and (2) immersed in an electrolytic solution of N species having concentrations c^*_i. Let us consider, for simplicity, a single electrochemical reaction at electrode (1) and a single electrochemical reaction at electrode (2), each having an equilibrium potential $E_{\rm eq,1}$ and $E_{\rm eq,2}$.

The cell potential under open circuit conditions (no current flow) can be defined as,

$$E_{\text{cell}} = E_{\text{eq},2} - E_{\text{eq},1} \tag{2.14}$$

Thus, if $E_{\text{cell}} > 0$, electrode (1) will act spontaneously as an anode and electrode (2) will acts spontaneously as a cathode. If $E_{\text{cell}} < 0$, electrode (1) will act spontaneously as a cathode and electrode (2) will act spontaneously as an anode. Hence, if an external load is connected between electrode (1) and (2) the system will behave as a galvanic cell, current flowing spontaneously from (1) to (2) if $E_{\text{cell}} > 0$ and spontaneously from (2) to (1) if $E_{\text{cell}} < 0$.

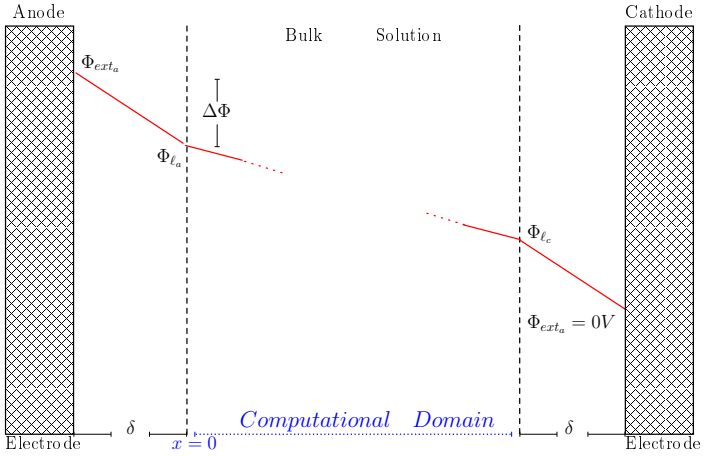

Figure 2.2: Potential distribution inside the domain.

Let us suppose that a potential difference V is applied between electrode (1) and (2) in a way such the potential at (1) is $V = \Phi_{\text{ext}}$ and the potential in (2) is zero (electrode (2) is grounded) see Fig. (2.2). Let us assume that even if current flows through the cell and the reactions proceed, the variation of concentrations is insignificant. Let us also assume that the electrode surfaces are uniformly accessible. In this case, the problem can be considered one-dimensional and the one-dimensional Laplace equation holds for the potential $\Phi(x)$ in the electrolytic solution,[1]

$$\frac{\partial^2 \Phi}{\partial x^2} = 0 \tag{2.15}$$

Under these conditions, the current density will be given by Ohm's law,

$$i = -\sigma \frac{\partial \Phi}{\partial x} \tag{2.16}$$

[1] The electrolytic solution is considered as the domain enclosed between the edges of the electrode double layer region

where the conductivity σ is,

$$\sigma = F^2 \sum_i z_i^2 u_i c_i^* \tag{2.17}$$

and under the above assumptions is constant throughout the electrolytic solution. The symbol u_i is used for the mobility of species i. The solution of Eq. (2.15) is,

$$\Phi(x) = a_1 x + a_2 \tag{2.18}$$

By combining Eqs. (2.18) and (2.16),

$$i = -\sigma a_1 \tag{2.19}$$

that is, the current density in the solution is independent of the position x. In order to determine a_1 and a_2 the appropriate boundary conditions must be defined.

Before proceeding to the definition of the boundary conditions, let us introduce that concept of *overpotential* of the electrode. Thus, overpotential is defined as the difference between the potential at metal phase of the electrode and the potential at the edge of the double layer, minus the equilibrium potential. Thus,

$$\eta_1 = \Phi_1 - \Phi(0) - E_{\text{eq},1} \tag{2.20}$$
$$\eta_2 = \Phi_2 - \Phi(l) - E_{\text{eq},2} \tag{2.21}$$

where $x = 0$ is the edge of the double layer of electrode (1) and $x = L$ is the edge of the double layer of electrode (2), see Figure (2.3). It is obvious that, under the above assumptions,

$$\eta_1 = \Phi_{\text{ext}} - \Phi(0) - E_{\text{eq},1} \tag{2.22}$$
$$\eta_2 = 0 - \Phi(L) - E_{\text{eq},2} \tag{2.23}$$

By using Eq. (2.18), we arrive to the following expressions for the overpotentials,

$$\eta_1 = \Phi_{\text{ext}} - a_2 - E_{\text{eq},1} \tag{2.24}$$
$$\eta_2 = -a_1 L - a_2 - E_{\text{eq},2} \tag{2.25}$$

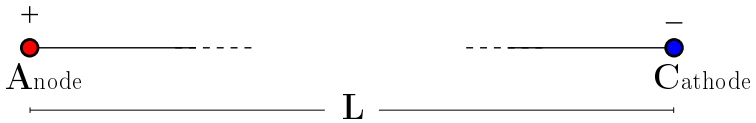

Figure 2.3: Domain for ODE problem.

Now, let us consider the following cases,

- **Very fast reactions**: Let us assume very fast reactions occurring with almost zero overpotentials, i.e. $\eta_1 = \eta_2 = 0$. Under this conditions, Eqs. (2.24) and (2.25) are written,

$$a_2 = \Phi_{\text{ext}} - E_{\text{eq},1} \tag{2.26}$$

$$a_1 = -\frac{\Phi_{\text{ext}} + E_{\text{cell}}}{L} \tag{2.27}$$

Thus, the potential distribution in the solution is,

$$\Phi(x) = -\frac{\Phi_{\text{ext}} + E_{\text{cell}}}{L}x + V - E_{\text{eq},1} \tag{2.28}$$

The current density is,

$$i = \frac{\sigma}{L}(\Phi_{\text{ext}} + E_{\text{cell}}) \tag{2.29}$$

Let us explore the above equations. If $V > E_{\text{cell}}$ then the slope of Eq. (2.28) is negative. Also, the current density i is positive. That is, current flows from electrode (1) to electrode (2), i.e. electrode (1) acts as an anode and (2) as a cathode.

If $V < E_{\text{cell}}$ then the slope of Eq. (2.28) is positive. In this case the current density i is negative. That is, current flows from electrode (2) to electrode (1), i.e. electrode (2) acts as an anode and (1) as a cathode.

Finally, we observe that if $\Phi_{\text{ext}} = -E_{\text{cell}}$ then the slope of Eq. (2.28) is zero. Apparently, $i = 0$, thus there is no current flow in the cell, even though a potential V is applied.

The potential drops in the system can be found by writing Eq. (2.29) in the following way,

$$\Phi_{\text{ext}} = \frac{L}{\sigma}i - E_{\text{cell}} \tag{2.30}$$

By taking into account that the specific conductivity is related to the solution resistance according to the formula,

$$\sigma = \frac{L}{AR} \tag{2.31}$$

then Eq. (2.30) is written,

$$\Phi_{\text{ext}} = IR - E_{\text{cell}} \tag{2.32}$$

where $I = Ai$ is the current and A the electrode surface. Equivalently,

$$\Phi_{\text{ext}} = \Delta\Phi_{\text{Ohm}} - E_{\text{cell}} \tag{2.33}$$

where $\Delta\Phi_{\text{Ohm}} = IR$ is the ohmic drop in the solution.

- **Linear kinetics**: Let us assume that the kinetics at electrode (1) obey a linear law,

$$\eta_1 = \frac{RT}{nFi_{0,1}} i = ki \tag{2.34}$$

and the kinetics at electrode (2) are fast, $\eta_2 = 0$.

Since $\eta_1 = \Phi_{\text{ext}} - \Phi(0) - E_{\text{eq},1}$, $\Phi(0) = a_2$ and $i = -\sigma a_1$ we obtain,

$$\Phi_{\text{ext}} - a_2 - E_{\text{eq},1} = -k\sigma a_1 \tag{2.35}$$

Since $\eta_2 = 0$, $\Phi(L) = a_1 L + a_2$ and $\Phi(L) = -E_{\text{eq},2}$ we obtain,

$$a_2 = -E_{\text{eq},2} - a_1 L \tag{2.36}$$

Combining the two equations above,

$$a_1 = -\frac{\Phi_{\text{ext}} + E_{\text{cell}}}{k\sigma + L} \tag{2.37}$$

$$a_2 = \frac{\Phi_{\text{ext}} + E_{\text{cell}}}{k\sigma - L} L - E_{\text{eq},2} \tag{2.38}$$

Thus, the potential distribution is,

$$\Phi(x) = -\frac{\Phi_{\text{ext}} + E_{\text{cell}}}{k\sigma + l}(x - L) - E_{\text{eq},2} \tag{2.39}$$

and the current density is,

$$i = \sigma \frac{\Phi_{\text{ext}} + E_{\text{cell}}}{k\sigma + L} \tag{2.40}$$

Apparently, when the reaction at the anode is very fast, $i_{0,1} \to \infty$, then $k \to 0$ and Eqs. (2.39) and (2.40) transform to Eqs. (2.28) and (2.29), respectively.

The potential drops in the system can be found from Eq. (2.40), similarly to the previous section,

$$\Phi_{\text{ext}} = \eta_1 + IR - E_{\text{cell}} \tag{2.41}$$

or equivalently,

$$\Phi_{\text{ext}} = \eta_1 + \Delta\Phi_{\text{Ohm}} - E_{\text{cell}} \tag{2.42}$$

We observe an additional potential drop corresponding to the overpotential at electrode (1).

- **Tafel kinetics:** Let us assume that the kinetics at electrode (1) obey Tafel kinetics,

$$\eta_1 = -\frac{RT}{a_1 nF}\ln i_{0,1} + \frac{RT}{a_1 nF}\ln i \tag{2.43}$$

and the kinetics at electrode (2) are fast, $\eta_2 = 0$. It is assumed that electrode (1) behaves as an anode.

The potential drops in the system will be given by an equation similar to Eq. (2.42), which can be written,

$$\Phi_{\text{ext}} = -\frac{RT}{a_1 nF}\ln i_{0,1} + \frac{RT}{a_1 nF}\ln i + IR - E_{\text{cell}} \tag{2.44}$$

or,

$$\Phi_{\text{ext}} = -\frac{RT}{a_1 nF}\ln I_{0,1} + \frac{RT}{a_1 nF}\ln I + IR - E_{\text{cell}} \tag{2.45}$$

where $I_{0,1} = Ai_{0,1}$ the exchange current at electrode (1). We observe that when the conductivity is very large then $R \to 0$ and the applied potential versus current curve (polarization curve) obeys Tafel kinetics. For finite R there is a deviation from Tafel kinetics due to the term $\Delta\Phi_{\text{Ohm}} = IR$. Similar results are obtained if electrode (1) is a cathode, by writing appropriately the Tafel kinetics, Eq. (2.43).

The condition at electrode (1) is written,

$$\Phi_{\text{ext}} - a_2 - E_{\text{eq},1} = -\frac{RT}{a_1 nF}\ln i_{0,1} + \frac{RT}{a_1 nF}\ln|-\sigma a_1| \tag{2.46}$$

The condition at electrode (2) is,

$$a_2 = -E_{\text{eq},2} - a_1 L \tag{2.47}$$

The above system of equations cannot be solved analytically. A numerical approximation can give a_1 and a_2 and thus an approximation of $\Phi(x)$.

- **Butler-Volmer kinetics**: In the case of Butler-Volmer kinetics at electrode (1),

$$i = i_{0,1}(e^{\frac{a_1 nF}{RT}\eta_1} - e^{-\frac{(1-a_1)nF}{RT}\eta_1}) \tag{2.48}$$

the coefficients a_1 and a_2 can be found by the condition at electrode (1),

$$-\sigma a_1 = i_{0,1}(e^{\frac{a_1 nF}{RT}(\Phi_{\text{ext}} - a_2 - E_{\text{eq},1})} - e^{-\frac{(1-a_1)nF}{RT}(\Phi_{\text{ext}} - a_2 - E_{\text{eq},1})}) \tag{2.49}$$

and the condition at electrode (2),

$$a_2 = -E_{\text{eq},2} - a_1 L \tag{2.50}$$

assuming $\eta_2 = 0$.

The above system must be solved numerically. Once the solution is known, $\Phi(x)$ and i can be determined, as a function of V.

- **Effect of double-layer**: In all the above examples, the double-layer capacitance was not taken into account. Assuming that electrode (1) behaves as a perfect capacitor with leakage, the current density on that electrode will be,

$$i = i_{\mathrm{F},1} + i_{\mathrm{c},1} \tag{2.51}$$

where $i_{\mathrm{F},1}$ is given by Eq. (2.48) and,

$$i_{\mathrm{c},1} = C_{\mathrm{dl},1}\frac{d(\Phi_{\mathrm{ext}} - \Phi(0))}{dt} \tag{2.52}$$

Thus, in order to determine a_1 and a_2, the following system of equations must be solver numerically,

$$\begin{aligned} -\sigma a_1 = i_{0,1}(e^{\frac{a_1 nF}{RT}(\Phi_{\mathrm{ext}} - a_2 - E_{\mathrm{eq},1})} - e^{-\frac{(1-a_1)nF}{RT}(\Phi_{\mathrm{ext}} - a_2 - E_{\mathrm{eq},1})}) \\ + C_{\mathrm{dl},1}\frac{d(\Phi_{\mathrm{ext}} - a_2)}{dt} \end{aligned} \tag{2.53}$$

$$a_2 = -E_{\mathrm{eq},2} - a_1 L \tag{2.54}$$

Once again, we assumed that the reaction at electrode (2) is very fast and thus $\eta_2 = 0$. We also ignore capacitance currents at electrode (2).

We must note that, in this case, the potential distribution must be written,

$$\Phi(x,t) = a_1(t)x + a_2(t) \tag{2.55}$$

that is, a_1 and a_2 do not depend on x but are functions of t.

In the case of Tafel kinetics (assuming electrode (1) is an anode),

$$-\sigma a_1 = i_{0,1}e^{\frac{a_1 nF}{RT}(\Phi_{\mathrm{ext}} - a_2 - E_{\mathrm{eq},1})} + C_{\mathrm{dl},1}\frac{d(\Phi_{\mathrm{ext}} - a_2)}{dt} \tag{2.56}$$

In the case of linear kinetics,

$$-\sigma a_1 = \frac{i_{0,1}nF}{RT}(\Phi_{\mathrm{ext}} - a_2 - E_{\mathrm{eq},1}) + C_{\mathrm{dl},1}\frac{d(\Phi_{\mathrm{ext}} - a_2)}{dt} \tag{2.57}$$

or, in general,

$$-\sigma a_1 = i_{\mathrm{F}}(a_2; \Phi_{\mathrm{ext}}) + C_{\mathrm{dl},1}\frac{d(\Phi_{\mathrm{ext}} - a_2)}{dt} \tag{2.58}$$

where $i_{\mathrm{F}}(a_2; \Phi_{\mathrm{ext}})$ an expression of the faradaic current.

2.2.2 Ordinary differential equation approach

In all the above examples, the concentration of the species in the electrolytic solution was assumed constant. In the case of varying concentrations, equation (2.58) is modified as follows,

$$C_{\mathrm{dl}}\frac{da_2}{dt} = \sigma\frac{-a_2 - E_{\mathrm{eq},2}}{L} + i_{\mathrm{F}}(a_2, c_1(0,t)\dots c_N(0,t); \Phi_{\mathrm{ext}}) \tag{2.59}$$

where now, the expression of the total faradaic current i_{F} depends also on the surface concentration of the reacting species, $c_i(0,t)$.

In order to evaluate the surface concentrations $c_i(0,t)$, the following assumption is introduced. We define a linear distribution of the concentrations near the electrodes on a distance δ and a constant value c_i^* in the bulk solution, for $i = 1, 2, \ldots, N$.

$$c_i(x,t) = \begin{cases} c_i(0,t) + \dfrac{c_i^* - c_i(0,t)}{\delta} x, & 0 \leq x \leq \delta \\ c_i^*, & x > \delta \end{cases} \tag{2.60}$$

A schematic representation of the concentration distribution near the anode is shown in Figure (2.4).

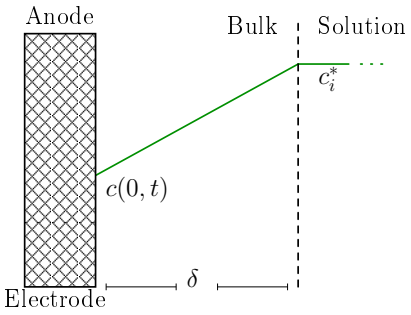

Figure 2.4: Concentrations distribution near the anode.

Under this assumption, and if we consider only one electroactive species, the mass balance equation at the anode is written,

$$\frac{dc_1(0,t)}{dt} = \frac{2D_1}{\delta^2}(c_1^* - c_1(0,t)) + \frac{2}{\delta}N_{\mathrm{migr},1} + \frac{2}{\delta}N_{\mathrm{F},1} \tag{2.61}$$

where $N_{\mathrm{migr},1}$ is the electromigration flux and $N_{\mathrm{F},1}$ the faradaic flux of the species.

For the faradaic flux, the Faraday law can be implemented, i.e.,

$$N_{\mathrm{F},1} = \frac{\nu_1 i_{\mathrm{F}}}{nF} \tag{2.62}$$

where ν_1 is the stoichiometric coefficient of the species and n the number of exchanged electrons. The electromigration flux, on the other hand, poses some additional problems. Nevertheless, two limiting cases are easy to handle. If the reacting species are minor, then the migration flux can be considered as zero. If the reacting species are more mobile that all other species, then the migration flux is almost equal to the total flux, i.e.

$$N_{\mathrm{migr},1} = \sigma \frac{-a_2 - E_{\mathrm{eq},2}}{z_1 F L} \tag{2.63}$$

The above system of ODEs can be solved numerically for a_2 and c_1 in order to determine the potential and concentration distribution at any t, if the faradaic current is defined. As mentioned before, the faradaic current depends on the mechanism and for a dissolution/passivation mechanism can be approximated by a function $i_{\mathrm{F}} = c_1(0) f(a_2; \Phi_{\mathrm{ext}})$ where [8],

$$f(\Delta\Phi_{\mathrm{a}}) = \alpha_1 \Delta\Phi_a \left(\frac{F}{RT} \Delta\Phi_{\mathrm{a}} - \alpha_2 \right)^2 \frac{F}{RT} \tag{2.64}$$

where $\Delta\Phi_{\mathrm{a}} = \Phi_{\mathrm{ext}} - a_2$.

A typical example of cycle voltammogram for the above model is presented in Figure (2.5). The parameter values are $\sigma = 4$ S/cm, $L = 10$ cm, $\delta = 0.01$ cm, $C_{\mathrm{dl}} = 10^{-5}$ F/cm^2, $D = 10^{-5}$ cm^2/s, $a_1 = 0.65$, $a_2 = 30$, $c_1^* = 0.001$ mol/cm^3, $z_1 = 1$, $n = 1$, $\nu = -1$. It can be observed that for relatively small values of applied potential the current increases until a limiting value. In the region from 0.68 to 0.76 V the current oscillates spontaneously. For large values of potential the current decreases due to "passivation".

The existence of autonomous oscillations is verified by plotting the current as a function of time for a fixed value of the applied potential within the oscillatory region. An example is presented in Figure (2.6) for $\Phi_{\mathrm{ext}} = 0.75$ V. It is evident that the oscillations are of relaxation type, where the current oscillates between a low value corresponding to a "passive" state and a high value corresponding to an "active" state.

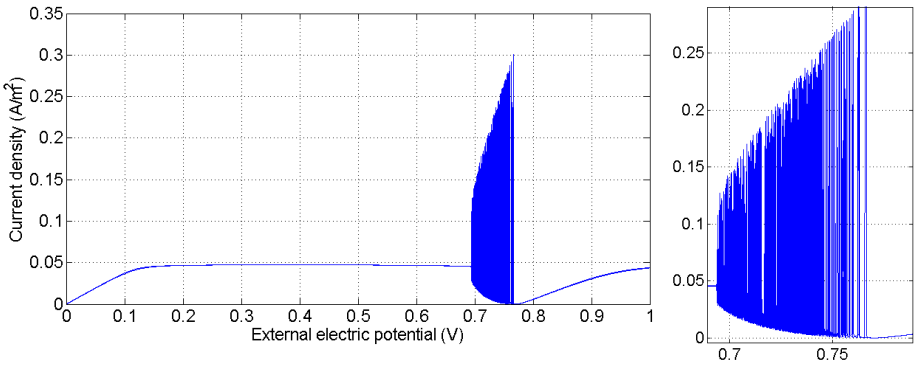

Figure 2.5: Cyclic voltammetry for the ODE model. Scan rate 1 mV/s.

The instabilities leading to oscillations can be identified from the corresponding bifurcation diagram, by considering Φ_{ext} as the bifurcation parameter and a_1 (which is proportional to the total current density). The bifurcation diagram is presented in Figure (2.7), where red lines correspond to stable steady states, black lines to unstable steady states and green lines to the minimum and maximum values of limit cycles. At the point corresponding to $\Phi_{\mathrm{ext}} = 0.68$ V a Hopf bifurcation occurs leading to oscillations. At $\Phi_{\mathrm{ext}} = 0.78$ V the oscillations disappear because the limit cycle merges with saddle point.

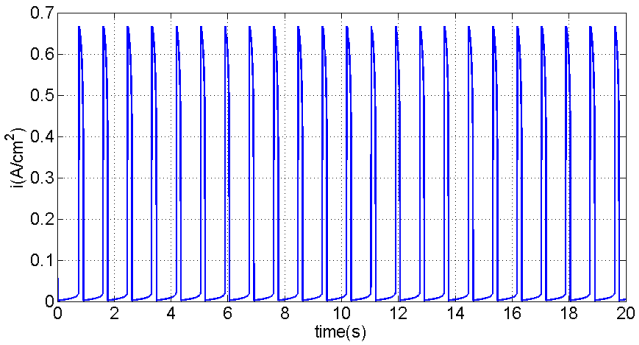

Figure 2.6: Time series of the current for the ODE model. $\Phi_{\text{ext}} = 0.75$ V.

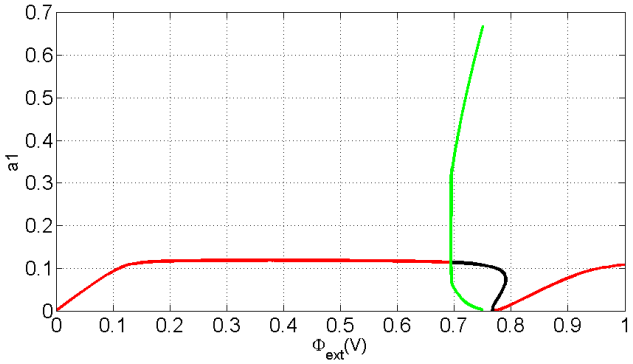

Figure 2.7: Bifuraction diagram for the ODE model.

2.2.3 Tertiary current distribution

The mass balance for the diluted species in the electrolytic solution is described by the following equation for three species:

$$\frac{\partial c_i}{\partial t} + \nabla \cdot \mathbf{N}_i = 0 \tag{2.65}$$

It is assumed that the flux can be described by the Nernst-Planck equation [15]. The transport depends on diffusion, convection and electromigration of ions. Also the direction of flux depends on the sign of z_i.

$$\mathbf{N}_i = -z_i u_i c_i \nabla \Phi_\ell - D_i \nabla c_i + c_i \mathbf{v} \tag{2.66}$$

The modeling of any electrolytic process requires the consideration of the three fundamental transport mechanisms diffusion, migration, and convection, which are the first, second, and third terms in the above equation. In this study, it is assumed that the fluid's velocity $\mathbf{v}$ is equal to zero. The Φ_ℓ denotes the electric potential in the solution. Ionic mobility, u_i in equation (2.66) was derived from the Einstein relation,

$$u_i = \frac{D_i}{RT} \tag{2.67}$$

In spite of the presence of charged species, the solution is electrically neutral except for within very thin layers adjacent to the electrodes whose effects are not taken into account in the present analysis. The constrain of electroneutrality reads,

$$\sum_{i=1}^{3} z_i c_i = 0 \tag{2.68}$$

which can be utilized to calculate c_3 algebraically.

The above system of four equations (three mass balance equations and electroneutrality) are sufficient to solve for the concentration distribution of three species and the potential distribution. The electric current is derived from the ionic flux according to the relation,

$$\mathbf{i} = F \sum_{i=1}^{3} z_i \mathbf{N}_i \tag{2.69}$$

2.2.4 Implementation of boundary conditions of concentrations and electrode potential

Let us denote the outward unit normal vector on the boundary of the computational domain. Then

Anode: On the boundary interface of the anode we assume a chemical reaction where only species (1) participate. Thus, on this boundary, the faradaic and capacitance currents are written as equation (2.70) and equation (2.71).

$$i_{\mathrm{F_a}} = c_1 f(\Delta\Phi_{\mathrm{a}}) \tag{2.70}$$

$$i_{\mathrm{C_a}} = C_{\mathrm{dl}} \frac{d(\Delta\Phi_{\mathrm{a}})}{dt} \tag{2.71}$$

The subscript a describes quantities on the anode. The function $f(\Delta\Phi_{\mathrm{a}})$ is a function of the potential difference of the applied potential on the anode $\Phi_{\mathrm{ext_a}}$ and the solution potential Φ_ℓ i.e. $\Delta\Phi_{\mathrm{a}} = \Phi_{\mathrm{ext_a}} - \Phi_\ell$ as defined in the previous section.

Thus, the total current density at the anode is expressed by the following equation,

$$i_{\mathrm{tot_a}} = i_{\mathrm{F_a}} + i_{\mathrm{C_a}} = \left(F \sum_{i=1}^{3} z_i \mathbf{N}_i \right) \cdot \mathbf{n}_i \tag{2.72}$$

where $\mathbf{N}_2 = \mathbf{N}_3 = 0$ because we assume that only the species (1) reacts on the anode.

The function $f(\Delta\Phi_a)$, given by equation (2.64), where the values of the constants α_1 and α_2 have been chosen after parametric studies of the problem, is presented in Figure (2.8). The value of α_1 ranges between 0.4-0.9.In general we have observed that as the distance between the electrodes increases, the value of α_1 must be larger. The parameter α_2 is always equal to 30. In the equation of capacitance current, the term C_{dl} is equal to 0.2 $\mathrm{F/m^2}$ and is associated with the electrical double layer capacitance.

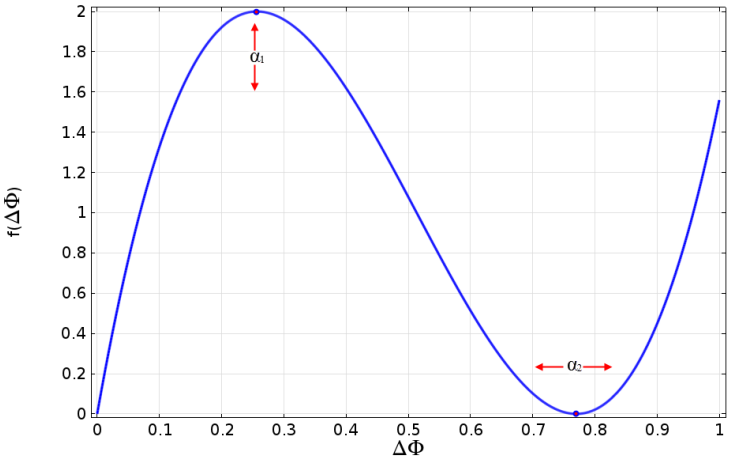

Figure 2.8: Graph of function $f(\Delta\Phi_a)$.

Cathode: To define the cathode of the electrolytic cell we use the expression (2.73) known as the Butler-Volmer equation.

$$i_{\mathrm{F_c}} = i_0 \left(e^{\frac{a_a F}{RT}\eta_{\mathrm{c}}} - \frac{c_2}{c_2^*} e^{-\frac{a_c F}{RT}\eta_{\mathrm{c}}} \right) \tag{2.73}$$

where the exchange current density $i_0 = 10^2$ $[\mathrm{A/m^2}]$, $a_{\mathrm{c}} = a_{\mathrm{a}} = 0.5$ denote the cathodic and anodic the charge transfer coefficients. We assume that the species c_2 reacts on the cathode, so the terms c_2 and c_2^* correspond to the concentration on the electrode and in the bulk. Finally the overpotential η_{c} is expressed as,

$$\eta_{\mathrm{c}} = \Phi_{\mathrm{ext_c}} - \Phi_{\ell_{\mathrm{c}}} - E_{\mathrm{eq_c}} = -\Phi_{\ell_{\mathrm{c}}} - E_{\mathrm{eq_c}} \tag{2.74}$$

We assume Φ_{ext_c} equal to zero, and E_{eq_c} equal to the equilibrium potential of the reaction. So the total current density on the cathode is,

$$i_{\mathrm{tot_c}} = i_{\mathrm{F_c}} = F \sum_{i=1}^{3} z_i \mathbf{N}_i \cdot \mathbf{n}_i \tag{2.75}$$

where the fluxes of species c_1 and c_3 are equal to zero because only species c_2 reacts on this boundary.

2.2.5 Initial conditions

As the problem is time dependant, we have to define initial conditions for the distribution of the concentrations. The solution is initially homogeneous (at equilibrium),

$$c_1 = c_2 = 1000\mathrm{mol/m}^3 \text{ for } t = 0 \tag{2.76}$$

the third species is calculated from electroneutrality, Eq. (2.68). We assume a zero value for electric potential field for t=0.

2.3 Definition of computational mesh

In this section we briefly describe the mesh used for solving the numerical scheme with finite elements. We have to keep in mind that in computational modelling we want a combination of reduced memory, CPU time and an accurate solution. In our problem, due to the fast oscillations of the current we need a quite fine space and time discretization. For all simulation cases the largest time step was set to 0.1 s where all the phenomenon lasts from 2000 s to 4000 s. At timesteps where the solution develops discontinuities we use the default options of Comsol 4.4, which discretizes freely the time until the solution converges.

2.3.1 Grid for 1D problem

In section (3.1) we describe the one dimension problem. There, we start the simulations with a uniform discretization of the computational domain. In order to obtain convergence we need a domain discretized with 185 elements, see Figure (2.9).

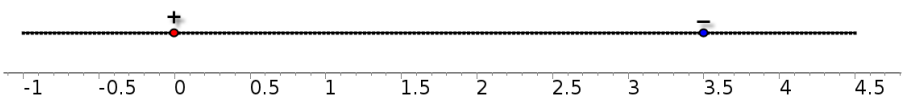

Figure 2.9: Uniform discretized grid.

From physical intuition, we consider that changes of the potential distribution in the solution will be rather smooth whereas, concentration variations will be drastic in the vicinity of the electrodes where the reactions occur. Thus, we create an non-uniform mesh with only 47 elements, see Figure (2.10). This second mesh, allow us to get accurate results using less memory and reducing the CPU time. The same idea is used for the problem of coupled electrodes in section (4.1). In that case we need 100 elements, the grid being finer near the electrodes and coarser everywhere else, see Figure (2.12).

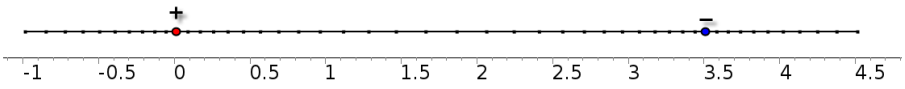

Figure 2.10: Non-uniform grid, finner near the electrodes.

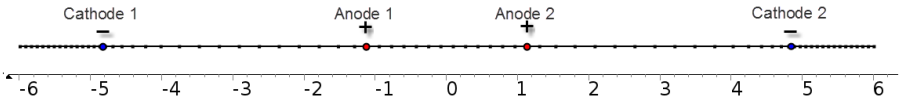

Figure 2.11: Non-uniform grid for the coupling case.

2.3.2 Grid for 2D problem

For the simulations in a two dimensional domain we assume a rectangular domain. Inside this domain we consider two cylindrical electrodes. Due to symmetry, and from the computational point of view, the electrodes can be considered as circles. The left circle is defined as the anode and the right as the cathode. This domain is described in detail in section 3.2. In order to discretize the computational domain we use the default triangular discretization of Comsol 4.4. Due to the preferences of domain the grid is finer near the electrodes and becomes coarser in the bulk of the solution (far from the electrode/electrolyte boundary). The number of triangular elements needed were 1817 and the computational time was about five hours in a medium performance personal computer.

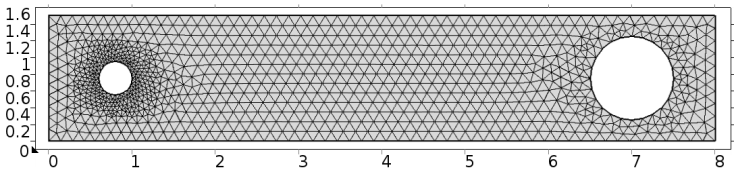

Figure 2.12: Non-uniform grid for the 2D model.

Chapter 3

A single oscillator

In this chapter we describe the computational solution of a one and a two dimensional problem concerning a single oscillator. We present parametric analyses for some of the parameters (e.g. the distance between the electrodes). Also we study the response of the system for different values of the applied potential and we present the distribution of the species concentrations and potential distribution in detail.

3.1 1D Problem

The simplest geometry is considered in a one dimensional domain. We assume a line with fixed length where we define two points A and C, the anode electrode on the left (A) and the cathode on the right (C) at a distance L, Figure (3.1). In the bulk solution we consider the existence of three species c_1, c_2 and c_3.

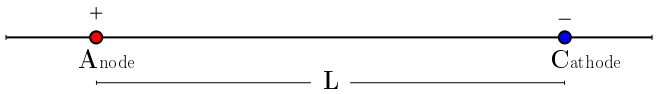

Figure 3.1: Computational domain fo 1D problem.

In order to find the region of the applied potential where the system becomes unstable we have to scan the potential. Therefore a triangle type function of the electric potential is implemented at the anode, see Figure (3.2). In this way we manage to produce the cyclic voltammogram, similarly to laboratory experiments.

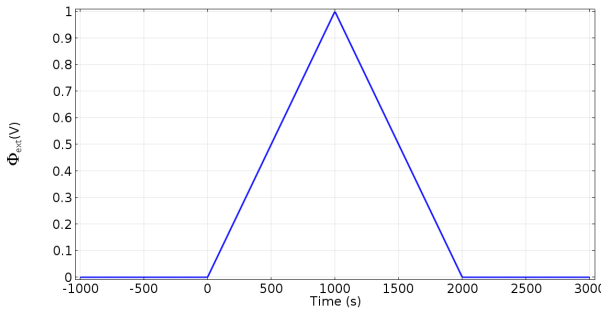

Figure 3.2: Triangular function for the applied (external) potential.

A typical graph corresponding to the above procedure is presented in Figure (3.3). The area which we are interested in, is the region where the behaviour of the system is not smooth. As we will see in the following, to get more precise information for that instability we have to scan the electrical potential with a smaller rate and make a parametric analysis for some parameters e.g. the distance L of the electrodes.

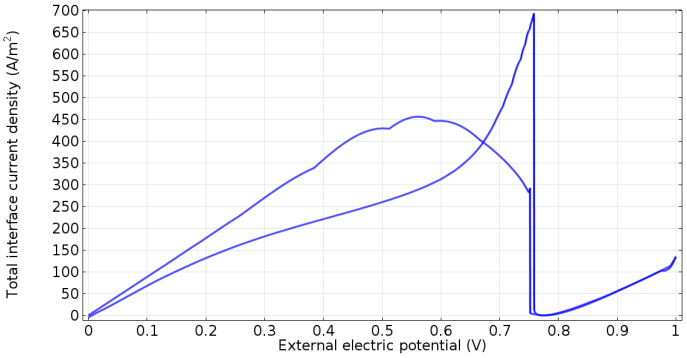

Figure 3.3: Cyclic voltammogram for high scan rate.

The emergence of oscillations depends on the distance between the electrode. The proper distance can be found by a parametric study for L, see Figure (3.4) and (3.5). It is clear that the optimal value for L is 3.5 cm, so the entire computational domain is 5.5 cm long. The anode electrode is located at the 0 point and the cathode at 3.5 cm. The domain is expanded 1 cm from each electrode, where the computational domain ends (the boundaries of the electrochemical cell).

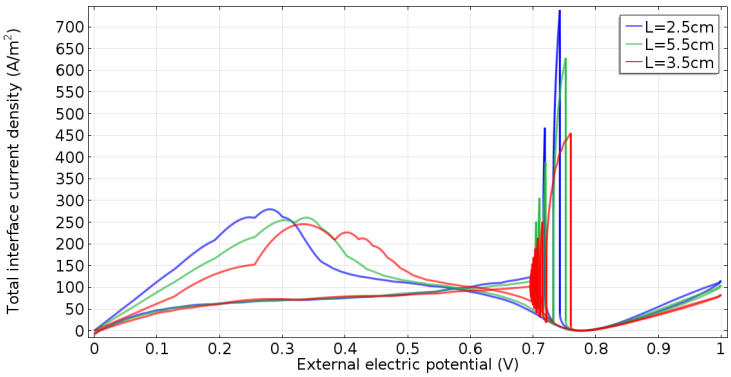

Figure 3.4: Parametric study for distance L.

The range of the applied electric potential Φ_{ext_a} in which the system oscillates is between 0.7 and 0.76 V as depicted in Figure (3.5). In order to observe the behaviour of the system we make a parametric study for fixed the values of Φ_{ext_a}. We chose three values inside the range of (0.7 V, 0.75 V). From Figure (3.6), we understand that for high values of the applied potential, the oscillations are more profound, that is, easier to observe.

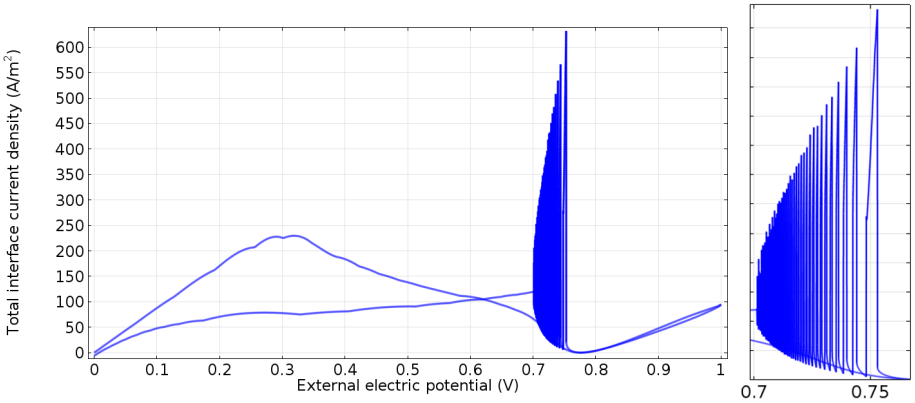

Figure 3.5: Cyclic voltametry for the optimal distance $L = 3.5$ cm.

There seems to be a conflict between these results and the cyclic voltammogram, as well as the bifurcation diagram presented during the ODE study of the system. Nevertheless, this discrepancy can be explained by taking into account the actual experiment which is modeled. Thus, this case corresponds to a potential-step experiment, starting from initial conditions where the concentrations have their bulk values throughout the domain and the potential gradient is zero. In order to observe the oscillations, both concentrations and potential have to follow a transient trajectory in the phase space which is finally attracted by the existing limit cycle.

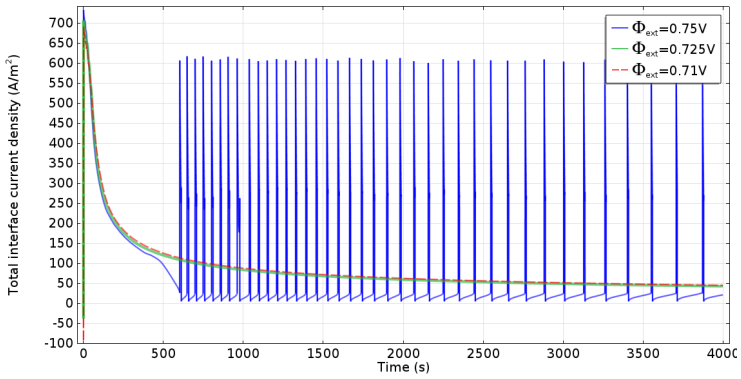

Figure 3.6: Parametric study for applied potential $\Phi_{\mathrm{ext_a}}$.

In order to bypass the problem of initial conditions being away from the limit cycle, the applied potential is scanned (as in cycle voltammetry), but in this case it is kept fixed at a desirable value, as presented in Figure (3.7). An additional benefit of this method is that we get realistic results using a coarser mesh. So it provides substantial saving in memory storage and CPU time, while preserving the accuracy of the solution.

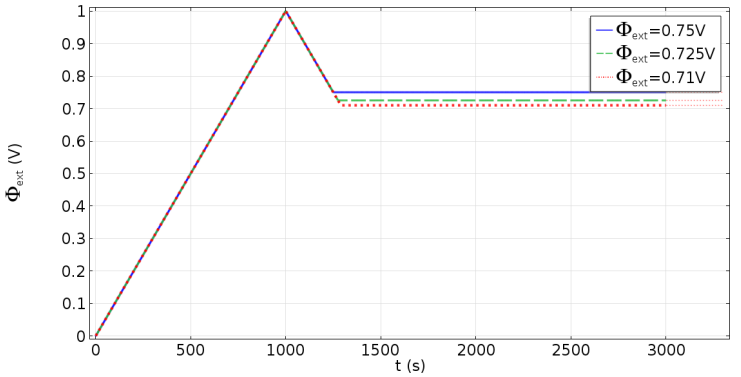

Figure 3.7: Scan of $\Phi_{\mathrm{ext_a}}$ where the final value of the potential is in the oscillatory region.

In Figure (3.8) the total current density at the anode is presented, for three different values of $\Phi_{\mathrm{ext_a}}$. Eventually, the optimal values of potential, where the current oscillations have long duration is at the upper limit of the oscillatory region.

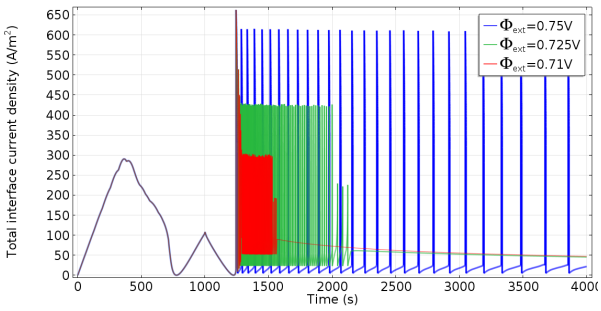

Figure 3.8: Parametric study for different values of the applied potential $\Phi_{\mathrm{ext_a}}$.

For $\Phi_{\mathrm{ext_a}} = 0.75$ V we can also calculate the fluctuations of concentrations of all species on the electrodes. In Figure (3.9), solids lines describe the variation of surface concentrations at the anode and dashed lines the surface concentrations at the cathode.

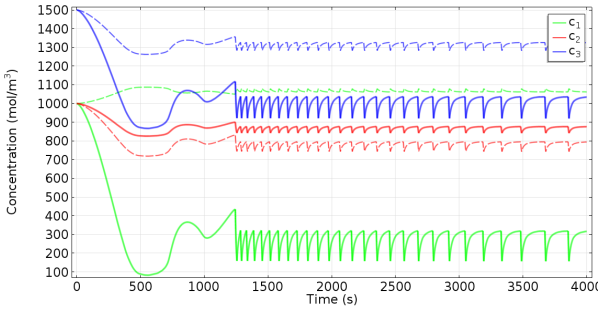

Figure 3.9: Fluctuations of the concentrations at the anode (solid lines) and the cathode (dashed lines).

In order to visualize the changes of all dynamic variables of the system during oscillations, we focus in a specific short time interval where the system oscillates, for example three spikes in [1240 s-1340 s], see Figure (3.10).

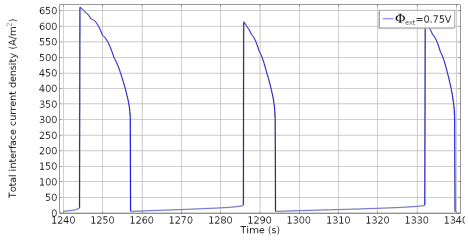

Figure 3.10: Current at the anode for a specific time interval.

In Figure (3.11) we present the distributions of potential and concentrations in the whole domain, in the left and right figure, respectively. The x axis donates the computational domain, where at the points 0 and 3.5 cm the electrode are located (anode and cathode, respectively). It is clear that during spiking, the distribution of the potential in the solution is more or less linear but fluctuates drastically, and the concentration of each species changes only within a small area close to the electrodes. These distributions are evident also from Figure (3.12), where a snapshot is presented for $t = 2000$ s.

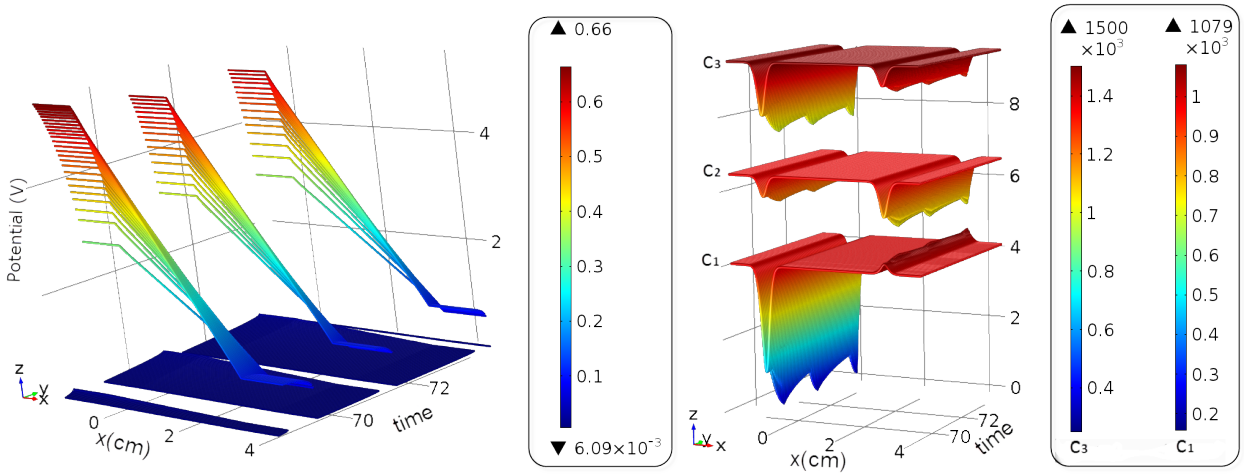

Figure 3.11: Distribution of potential and concectrations for a specific time.

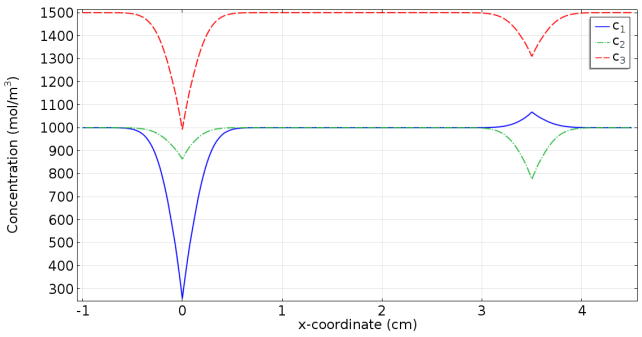

Figure 3.12: Concentration distribution of all species at $t = 2000$ s.

3.2 2D Problem

For the two dimensional problem we assume a rectangle domain a size of 1.5 cm (at x direction) and 8 cm (at y direction). Inside the rectangle we place the electrodes at a distance $L = 6.5$ cm. The distance L has been chosen as the optimal distance in order to have oscillations of long duration, similarly to the 1D problem. During the laboratory experiments, electrodes of different dimensions are used, therefore the reactive areas of electrodes have different size. We consider that the cathode area must be at least 2 times larger than the anode area, [14, 5]. Thus, we suppose two cylindrical electrodes (cycles due to symmetry) where the cathode radius is two and a half times bigger than the anode, see Figure (3.13).

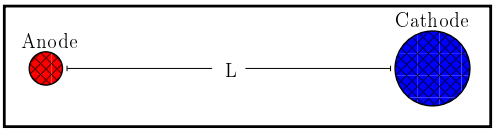

Figure 3.13: Computational domain for 2D problem.

The potential region where the system develops instability is located, once again, by scanning the potential. We observe a behaviour similar to the 1D problem, as can be seen in Figure (3.14).

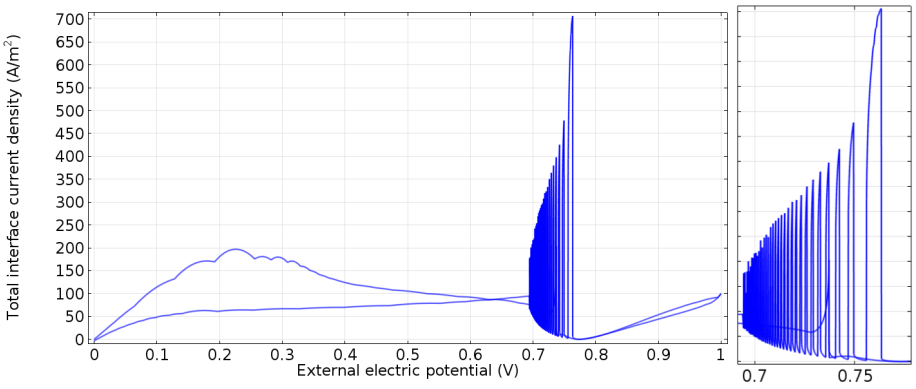

Figure 3.14: Cyclic voltammetry in the 2D case.

The potential region where we observe autonomous oscillations is located between the values of 0.7 and 0.75 V. From the parametric study of the potential, the applied potential value of $\Phi_{\text{ext}_a} = 0.75V$ is chosen, since for this value the oscillations have long duration. Thus, scanning for three different values of external potential Φ_{ext}, we observe that the period depends on the applied potential, see Figure (3.15). The different behaviour of the system is visualized better in figure (3.16), where we focus in a specific short time interval.

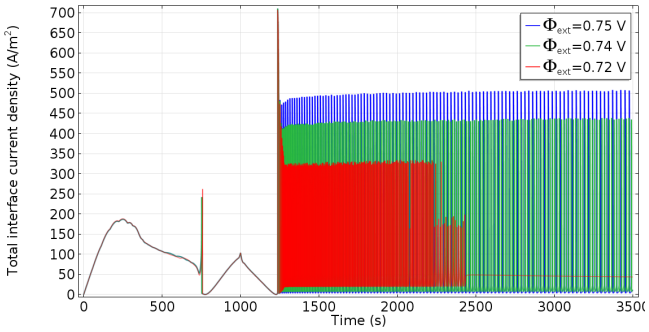

Figure 3.15: Parametric for the applied potential $\Phi_{\mathrm{ext_a}}$.

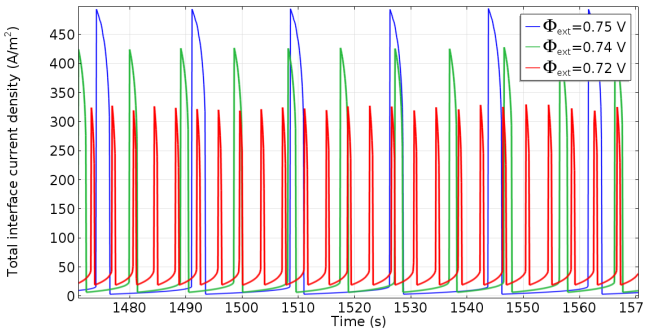

Figure 3.16: Parametric for the applied potential $\Phi_{\mathrm{ext_a}}$, for a short time interval.

A contour figure for the distribution of potential and the normalized vector of current density is presented in Figure (3.17) for $\Phi_{\mathrm{ext_a}} = 0.75$ V. As in the 1D model, the potential increases near the anodic electrode (left cycle), it follows a linear distribution between the electrodes and it takes values near zero on the cathodic electrode (right cycle). The vectors of current density are always perpendicular to the contour lines of the potential, and the direction of the current is from the anode to the cathode, as expected. A 3D representation of the above variables is presented in Figure (3.18).

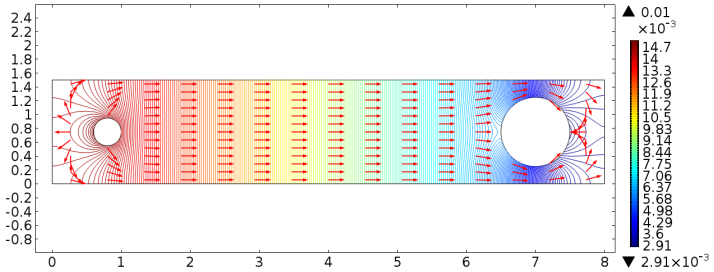

Figure 3.17: Contour of the potential Φ_ℓ and vectors of current density, $t = 3000$ s.

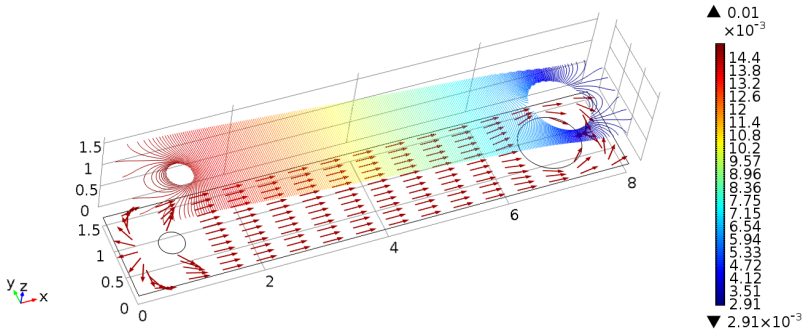

Figure 3.18: Contour of the potential and vectors of the current density, $t = 3000$ s.

As mentioned in section (2.2.3), the species c_1 are consumed at the anode. The species c_2 are consumed at the cathode and the third species c_3 move in order to fulfil the electroneutrality condition, see Figure (3.19).

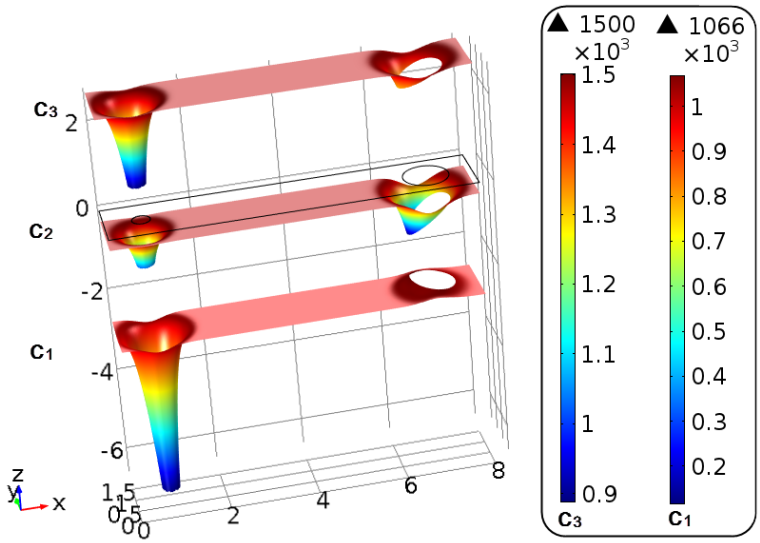

Figure 3.19: Distribution of the concentrations in the domain, $t = 3000$ s

As mentioned before, the movement of ions in the electrolytic solution is due to diffusion and electromigration. Diffusion fluxes are caused to concentration gradients. The concentrations gradients for all species are shown in Figure (3.20). It can be observed that concentration gradients for all species near the anode are positive whereas they are negative for species c_2 and c_3 and positive for species c_1 near the cathode.

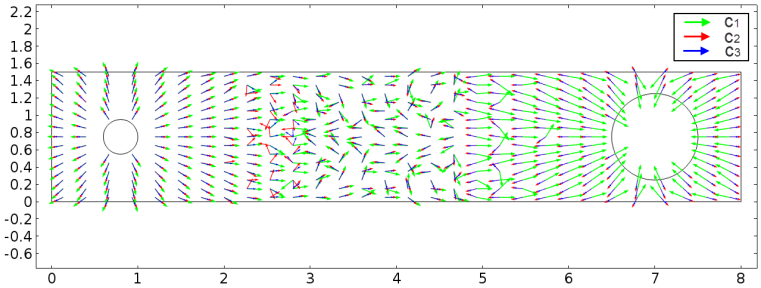

Figure 3.20: Concentration gradients in the domain, $t = 3000$ s

The diffusion fluxes are presented in Figure (3.21). As expected the direction of the flux is the opposite of the direction of the gradient, as expressed from Fick's law.

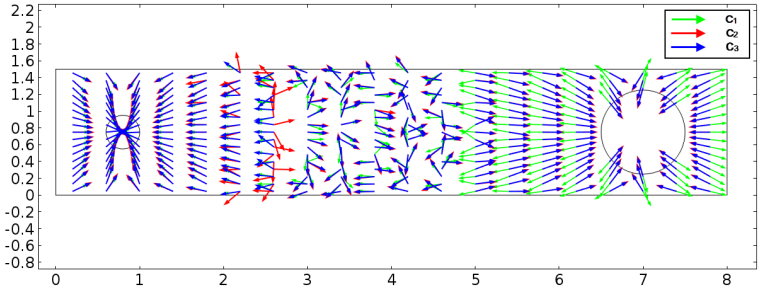

Figure 3.21: Diffusion flux in the domain, $t = 3000$ s

The electromigration flux is presented in figure (3.22). It is obvious that the migration flux of species c_1 and c_2 is from the anode to the cathode whereas for species c_3 is the opposite. This is to be expected since positive ions move from regions of high potential to regions of low potential and negative ions move from regions of low potential to regions of high potential.

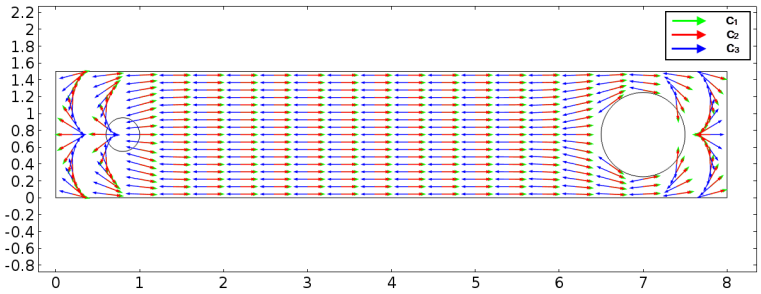

Figure 3.22: Electromigration flux in the domain, $t = 3000$ s

The advantage of the simulation of the two dimensional model is that we can get informations in particular areas of computational domain. In this paragraph we study the changes of potential and concentrations on the surface of electrodes. For a time period corresponding to a single spike we choose four time instances, t_1=1849.6 s,t_2=1849.9 s,t_3=1850.2 s and t_4=1850.5 s, see left Figure (3.23). On the right sketch of the same figure we define how we measure the arc length of the electrode in degrees. The zero degree is located on the right side of the anode. This side of the anode is the one facing the cathode. The 180^o are facing the left boundary of the electrochemical cell. For the cathode we use the mirrored image of the (3.23), i.e. the zero is on the left side of the cycle with face at the anodic electrode.

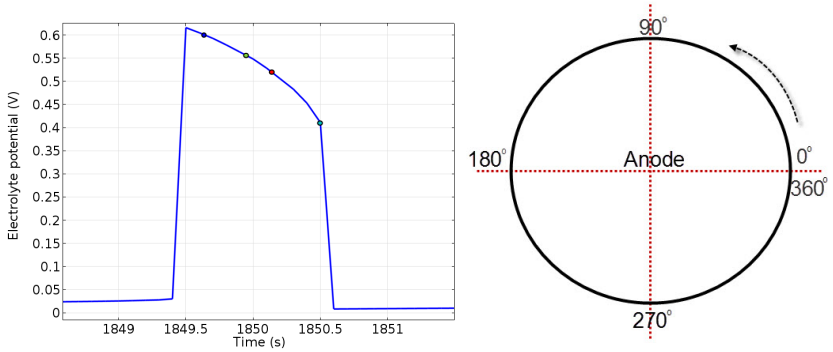

Figure 3.23: Four selected timesteps during one spike (left), definition of the arc lenght on the anode (right).

In Figure (3.24), we present the potential distribution on the surface of the anode. It is evident that the distribution is not homogeneous. The potential is higher in the region of the surface facing the cathode and lower in the region the cell boundary. Moreover we can observe that, at list for this four time instances the potential values are changing but the distribution remains the same.

A similar behaviour is observed at the cathode where the change of the values of the potential are not so profound due to the low value of the overpotential of this electrode (this electrode behaves as an ideally non polarized electrode), see Figure (3.25).

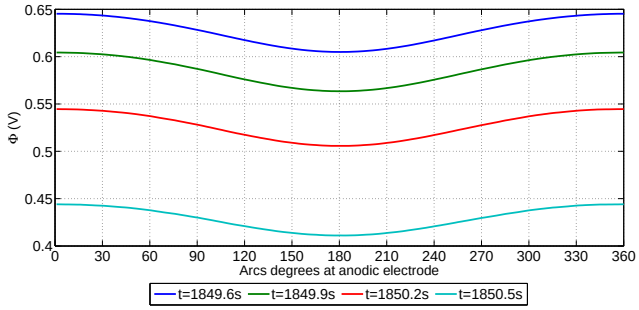

Figure 3.24: Distribution of the potential on the anodic surface.

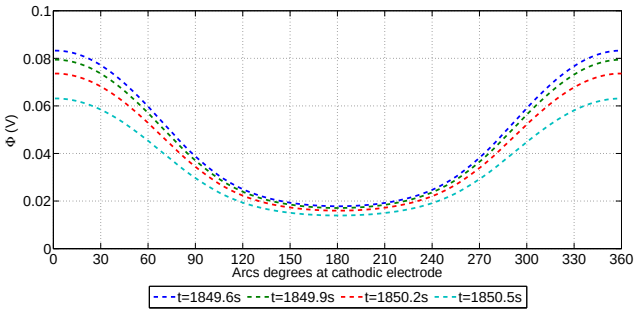

Figure 3.25: Distribution of the potential on the cathodic surface.

In Figure (3.26), we present the corresponding concentration distribution of species c_1. In this case we observe a non homogeneous distribution together with localized profound inhomogeneities. The nature of this localized inhomogeneities is difficult explain due to the luck of corresponding experimental data, [2, 1, 11]. Modification of the computational mesh did not result smoother distribution, thus this behaviour cannot be attributed easily to numerical accuracy.

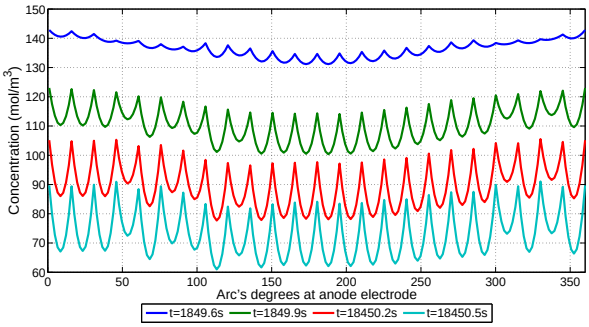

Figure 3.26: Distribution of the concentration of c_1 on the anodic surface.

Chapter 4

Coupled Electrodes

In the section we present the case of two coupled electrode pairs immersed in a common electrolytic solution. Was assume that the electrode pairs are electrically isolated and the only communication medium is the electrolytic solution. We study the interactions between the electrode pairs and their influence on the geometry of the network. The study is restricted to the 1D where the CPU memory requirements and computational time are not extreme.

4.1 C_1A_1 - A_2C_2 networks

We suppose an one dimensional domain (point 0 is the middle point of the domain). Anode_1 is located at the point -1.3 cm and the Anode_2 at 1.3 cm, i.e. the distance between the anodes is $d = 2.6$ cm, see Figure (4.1). The cathodic electrodes are located a at a distance of $L = 3.5$ cm from the corresponding anodes, as it has been described in section 3.1. We denote this network as C_1A_1 - A_2C_2 and we expect interaction between the oscillators through the neighbouring anodes.

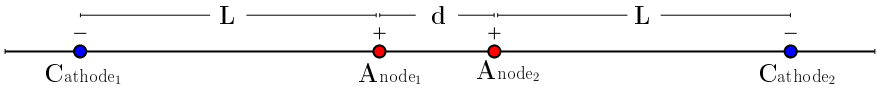

Figure 4.1: Computational domain of C_1A_1-A_2C_2.

4.1.1 In-phase synchronization

Fist we have to locate the applied potential region in which the network oscillates. Following the same procedure are before, the potential is scanned, similarly to a cyclic voltametry experiment. In figure (4.32), we present the result the cyclic voltammogram, and we notice that the couples oscillate simultaneously in the region $\Phi_{\text{ext}} \in [0.7 - 0.76]$.

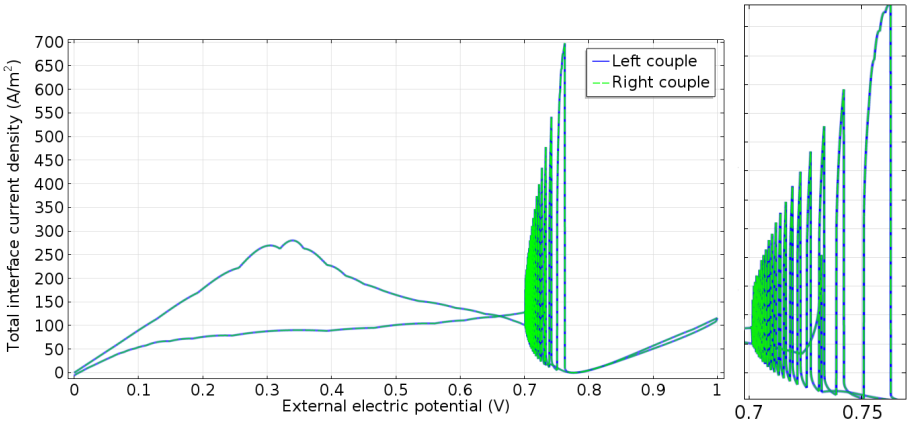

Figure 4.2: Cyclic voltammetry for a C_1A_1 - A_2C_2 network.

The cyclic voltammetry calculations indicate that the network is synchronized in-phase, that is, both oscillators oscillate simultaneously with the same period and zero phase difference. In order to understand how these pairs interact we implement a different function for the applied potential on each electrode pair. At every case, the potential of left pair C_1A_1 is considered are reference (blue diagrams) and we alter the right pair A_2C_2 (green diagrams). So we keep the same scan rate for each electrode, but at the end of the scan we set pair (1) at potential $\Phi_{\text{ext}} = 0.735$ V and pair (2) at potential $\Phi_{\text{ext}} = 0.735$ V unit $t = 2000$ s. For $t > 2000$ s the potential of pair (2) is changed to $\Phi_{\text{ext}} = 0.75$ V, see Figure (4.3).

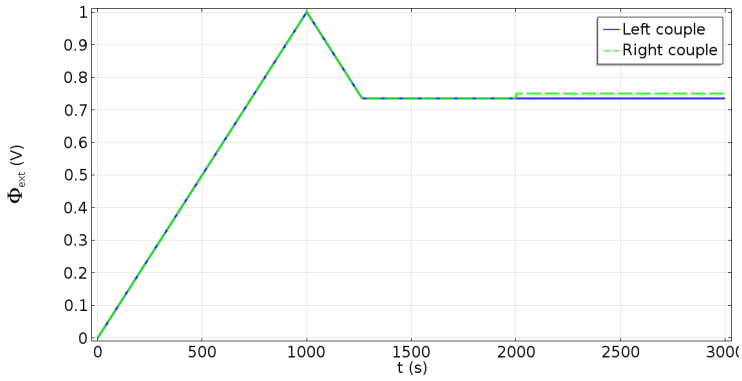

Figure 4.3: Scan of Φ_{ext_a} for the C_1A_1 - A_2C_2 network.

In Figure (4.4) the total current densities are presented for each pair. The green dashed curve represented current density at the anode of pair (2) (**Anode$_2$**) and with blue solid line the current density at the anode of pair (1) (**Anode$_1$**). Until the first 2000 s the oscillators are synchronized in-phase, At $t = 2000$ s the applied potential is changed from 0.735 V to 0.75 V of pair (2) and the amplitude as well as the period of the oscillations increase, as expected. The instance where this change of the potential is implemented is observed also in the right figure of (4.4). It is observed that the period as well as the amplitude of pair (1) also increases due to coupling. Due to the increase of period, the electrode pairs still oscillate in-phase but due to the difference of the amplitude, the wave-forms are not identical. This can be seen more easily if we plot the difference between the values of total current densities, equation (4.1). We can observe the evolution of this difference in Figure (4.5).

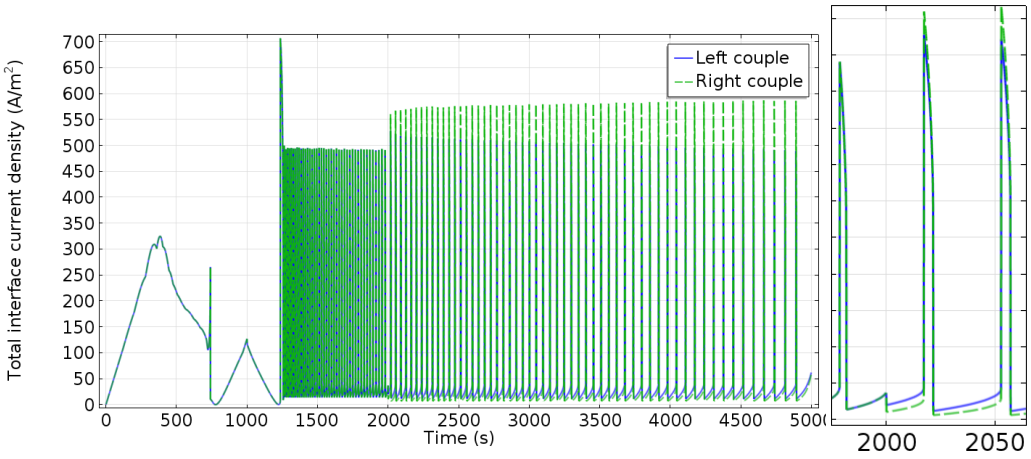

Figure 4.4: Total current density at the anode of pair (1) and (2).

$$\boxed{\Delta i_{tot} = i_{right} - i_{left}} \tag{4.1}$$

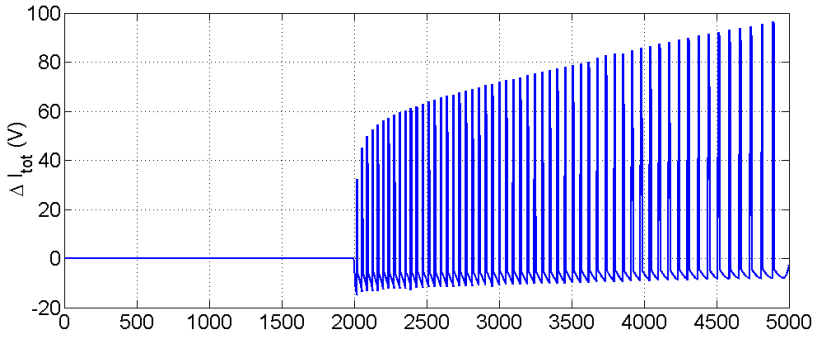

Figure 4.5: Difference of total current densities of the anodes of pair (1) and (2).

The next set of calculations concern the opposite change of the applied potential. Thus, we start from a higher value of applied potential and decrease it at lower value. The potential is scanned to the value $\Phi_{\text{ext}_1} = 0.75$ V and at $t = 2000$ s we set the potential of **Anode**$_2$ at $\Phi_{\text{ext}_2} = 0.735$ V, see Figure (4.6).

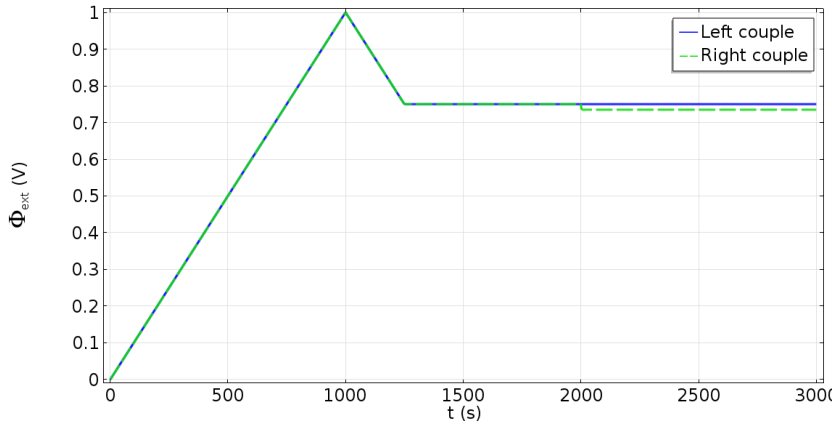

Figure 4.6: Scan of Φ_{ext_a} for the C_1A_1 - A_2C_2 network.

From Figure (4.7), we notice that, initially the oscillators are synchronized. At $t = 2000$ s, the amplitude of pair (2) decreases due to the lower value of the applied potential. The wave-forms of the oscillators are different, but they remain synchronized in-phase. If we represent the the differences of the current densities of this case (red line) and the previous case (blue line), they are exactly the same, see Figure (4.8).

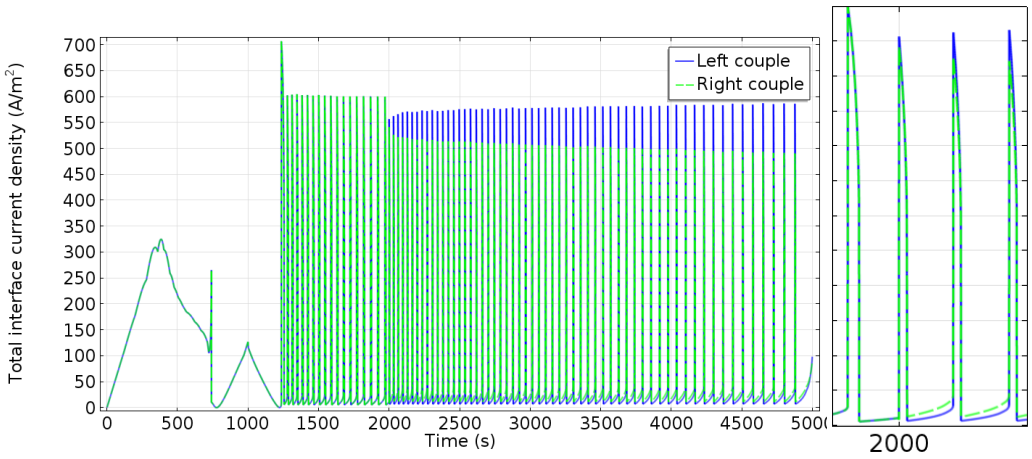

Figure 4.7: Total current densities of two anodes for the C_1A_1 - A_2C_2 network.

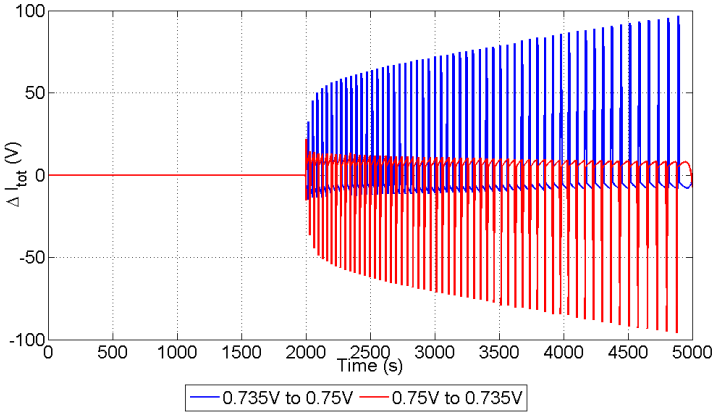

Figure 4.8: Difference of total current densities of the anodes of pair (1) and (2).

The influence of the initial conditions on this network of identical oscillators is examined by scanning the each potential with different rates and setting the final constant potential to the same value, as presented in Figure (4.9). So the scan the pair (1) (blue) reaches the value of $\Phi_{ext} = 0.75$ V at 1250 s while the rate of pair (2) (green) reaches the same value at 1875 s.

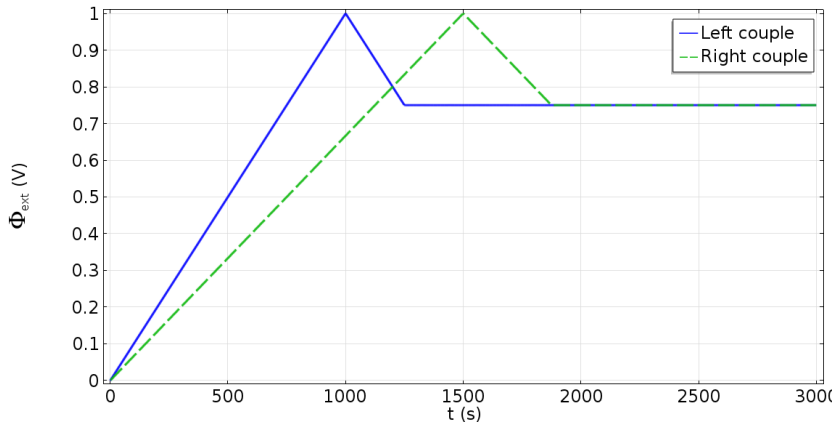

Figure 4.9: Scan of Φ_{ext} for the C_1A_1 - A_2C_2 network with different rates.

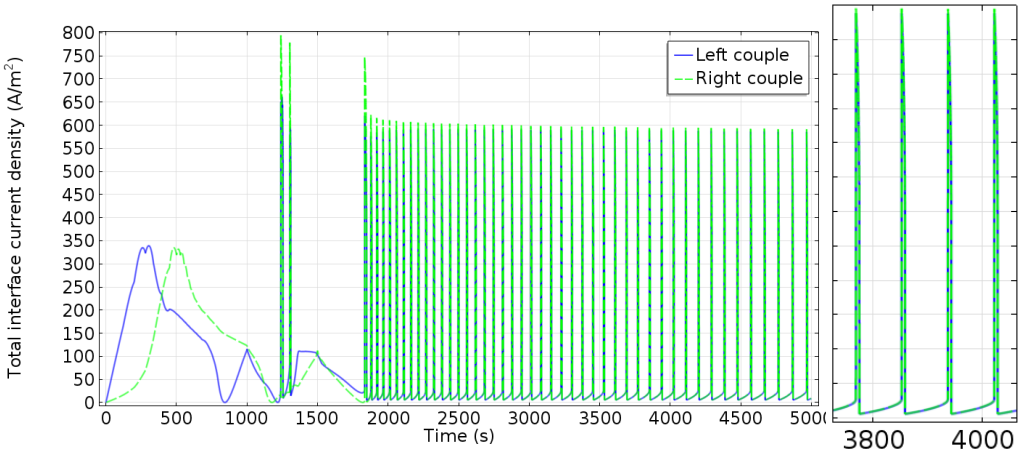

Figure 4.10: Total current densities of the anodes of pair (1) and (2).

We can draw some conclusions on the synchronization observed from the figure (4.10). It is clear that in the beginning of the simulation the pair (1) (blue) has an expected delay. At 1250 s this pair, which enters the oscillatory area, tries to oscillate and it drifts the other pair without success. Instead, at $t = 1875$ s, when pair (2) (green) starts to oscillate, pair (1) (blue) starts a simultaneous oscillation. Calculating the difference of the values of two currents, Eq. (4.1) we notice a synchronized behaviour in time, see Figure (4.11) where the two oscillators become almost identical.

The evolution of the potential and the ionic current during synchrony can be seen in Figure (4.12). Here, we plot the distribution of the potential and the flow of ionic current in the time interval from 3800 s to 4000 s, that is, during two oscillatory peaks. We observe that during the "passive" state of the oscillations

(low current density at step 347), there is a small potential difference between Anode1 and Anode2. Due to this small potential different, the ionic current between the interacting anodes is almost zero (no arrows in the region between the anodes). Small ionic currents flow between Anode_1 and Cathode_1 and Anode_2 and Cathode_2. During the oscillatory spike (in the interval between steps 348 and 349), the ionic current between Anode_1-Cathode_1 and Anode_2-Cathode_2 is large, due to the developed potential difference between these electrodes. Additionally, a potential difference is developed between Anode_1 and Anode_2 and current flows from the first to the second. Thus, it can be concluded that the transmitted information between the two oscillators is the ionic current between the two anodes, which is induced during the "active" state of the oscillations.

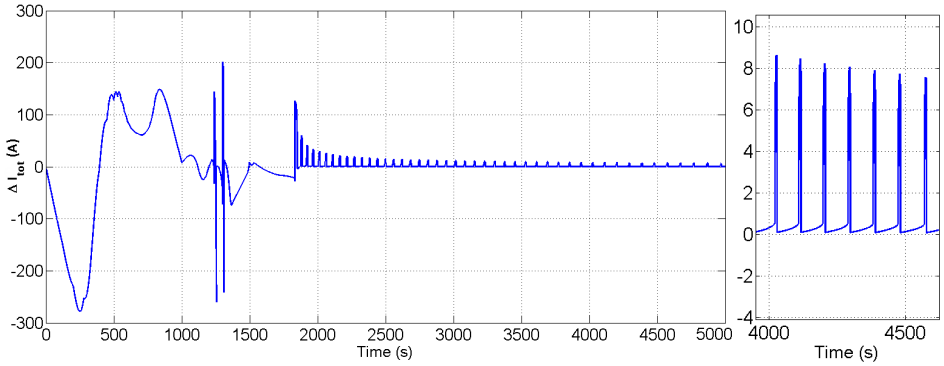

Figure 4.11: Difference of total currents of two anodes.

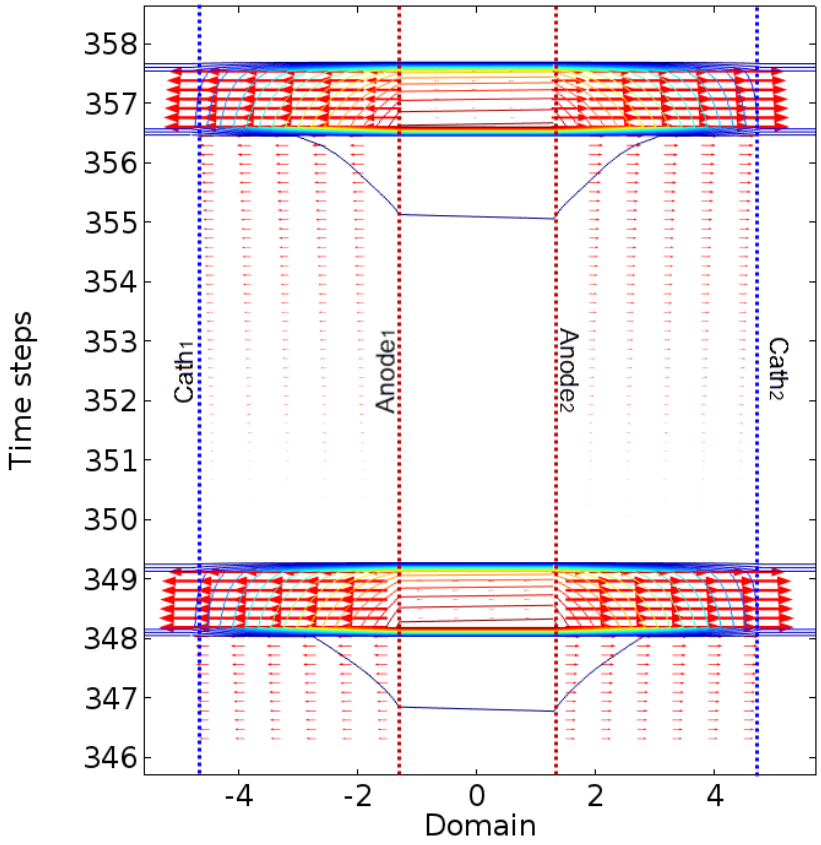

Figure 4.12: Contour of potential and vectors of the ionic current density in the computational domain during oscillations.

4.2 A_1C_1 - A_2C_2 networks

In this case the distances are $L = 3.5$ cm and $d = 2.6$ cm but the configuration of pair (1) is altered, as shown in Figure (4.13). So, $Anode_1$ is located at point -4 cm, $Cathode_1$ at -1.3 cm, $Anode_2$ at 1.3 cm and $Cathode_2$ at 4 cm. We denote this network as A_1C_1 - A_2C_2 and expect interaction through $Cathode_1$ and $Anode_2$.

In Figure (4.33) we present the cyclic voltammogram. We observe a different behaviour for each couple. Moreover, the oscillatory region has been shifted anodically, in comparison with the previous results.

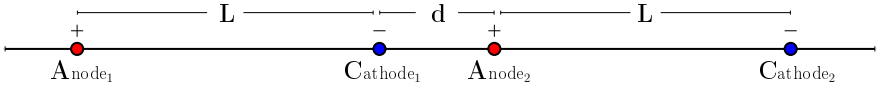

Figure 4.13: Computational domain of the A_1C_1-A_2C_2 network.

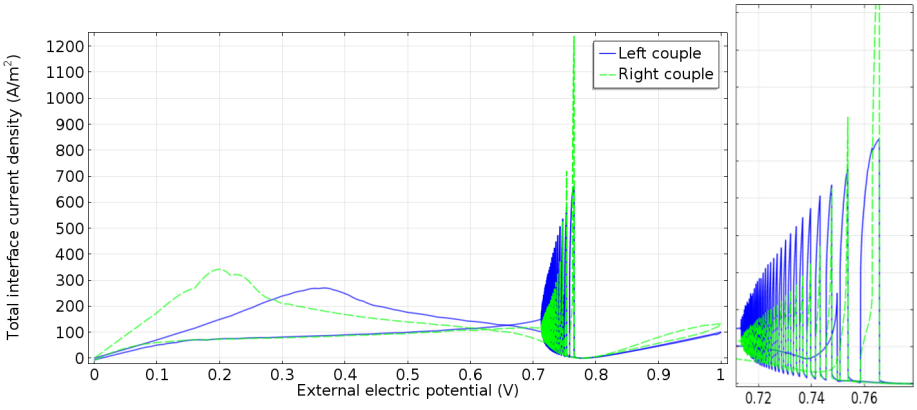

Figure 4.14: Cyclic voltammetry scanning for the A_1C_1-A_2C_2 network.

In order to clarify this response, we a computation by keeping the pair 1 (blue) in a fixed potential 0.75 V while the potential of pair (2) (green) is scanned. In the Figure (4.15) it is shown how the pair with a potential value in the oscillatory region affects the other pair, whose potential scanned. For example, in the to diagram of Figure (4.16), we have focused in the time interval form 1250 - 1660 s where pair (2) (green) has a potential in the region from 0.8 to 1 V. In this area, pair (1) (blue) tends to "passivite" pair one. Then, when pair (2) enters the oscillatory region, the oscillators tend to synchronize.

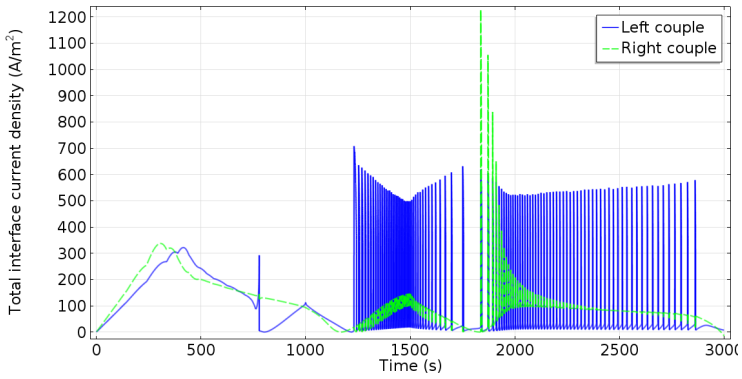

Figure 4.15: Cyclic voltammetry for pair (2) (green) and fixed potential for pair (1) (blue) in the A_1C_1-A_2C_2 network.

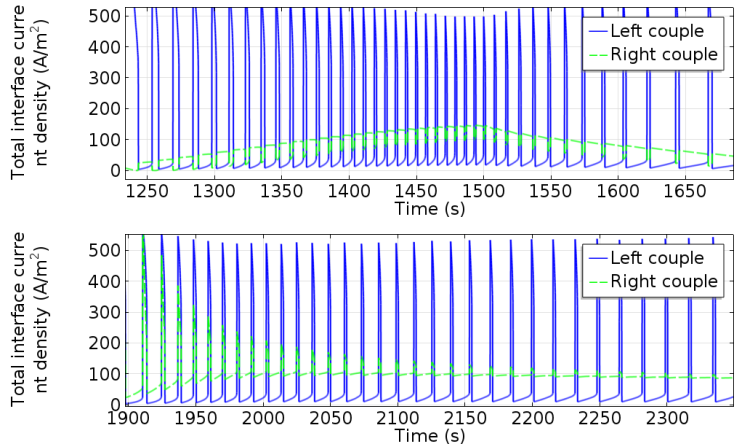

Figure 4.16: Cyclic voltammetry for pair (2) (green) and fixed potential for pair (1) (blue) in the A_1C_1-A_2C_2 network for specific time regions.

As in the previous geometry, in this section we study the case in which we keep the potential fixed at pair (1) equal to 0.735 V and for pair (2) we start from the 0.735 V and at time of 2000 s we switch it at 0.75 V, see Figure (4.17). Using this geometry (A_1C_1-A_2C_2), we notice that the whole system follows the characteristics of the couple with the fixed potential, i.e the oscillations cannot last longer than 2800 s when pair (1) turns from oscillations to a steady state.

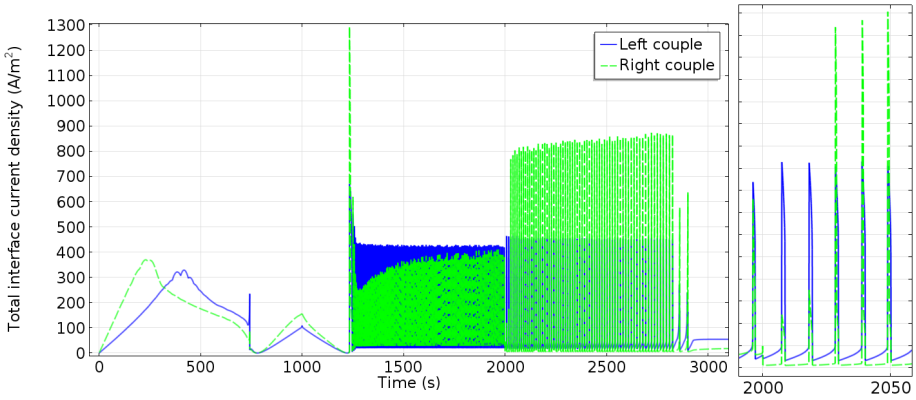

Figure 4.17: Total current densities of two anodes for the A_1C_1-A_2C_2 network.

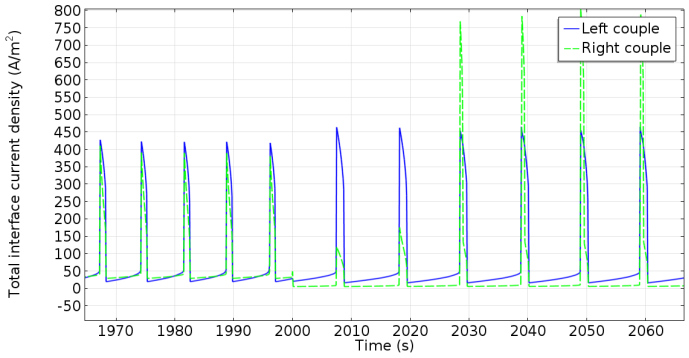

Figure 4.18: Oscillations during the transition of the potential of pair (2) (green) to higher values for the A_1C_1-A_2C_2 network.

On the other hand, when the value of pair (1) is higher, $\Phi_{\text{ext}} = 0.75V$ and we change the value of pair (2) from the 0.75 to 0.735 V we notice that the system remains on sustained oscillations, see Figure (4.19) and (4.20).

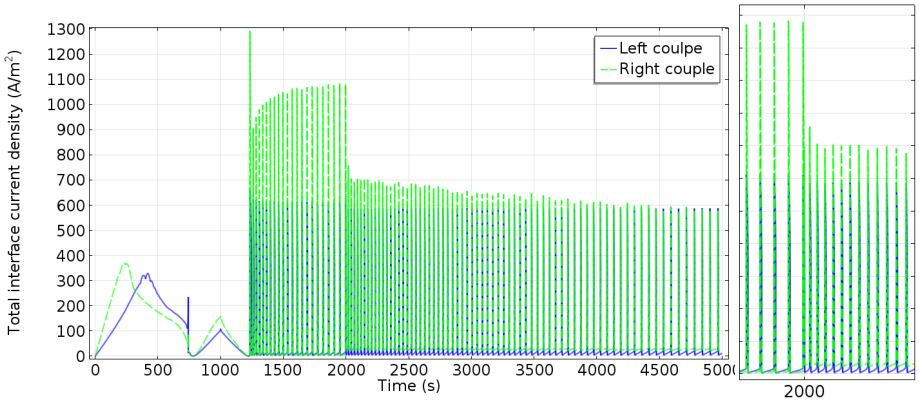

Figure 4.19: Total current densities of two anodes for the A_1C_1-A_2C_2 network.

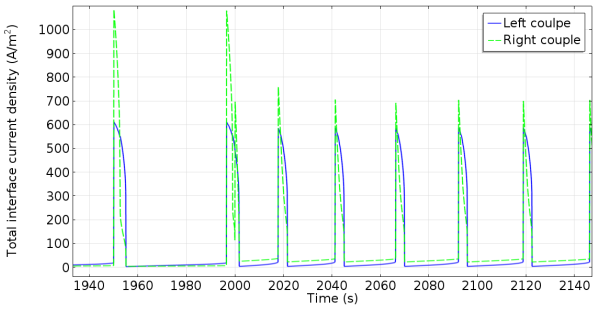

Figure 4.20: Oscillations during the transition of the potential of pair (2) (green) to higher values for the A_1C_1-A_2C_2 network.

By calculating the difference Δi_{tot}, the conclusions of the previous observations become evident. The blue line presents the case where the system goes from a lower potential to a higher, and turns to a steady state at 2900 s. The red line describes the second case when we change the potential of a higher value to a lower. From the time of 2000 s, where we make the change, the system tries to stabilize the spikes and finally the network is synchronized. The negative values is due to the fact that the current of pair (2) is larger than that of pair (1), see Figure (4.21).

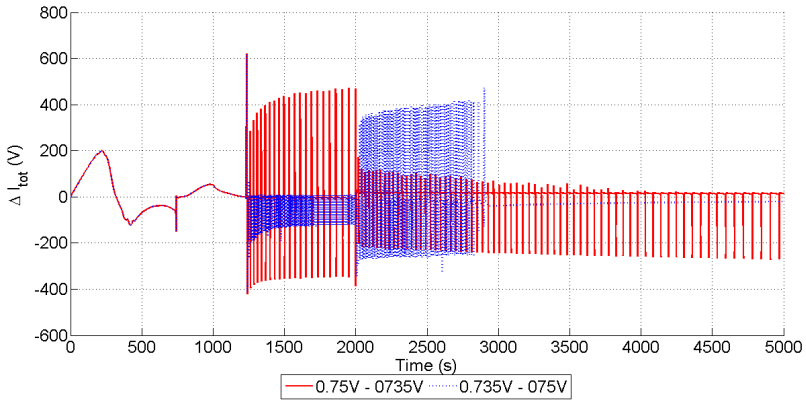

Figure 4.21: Difference of total current densities of the two anodes of pair (1) and (2).

In this case we study how the system is effected when we keep the same potential at both electrode pairs but we scan it with different rate. In this way, the effect of initial conditions is explored. So, we scan the pair (2) with a slower rate than that of pair (1).

In Figure (4.22) we observe that at $t = 1250$ s pair (1) (blue) starts to oscillate for applied potential $\Phi_{\text{ext}} = 0.75$ V. At the same time pair (2) (green) is at higher potential and it is affected by pair (1). At $t = 1800$ s pair (2) has almost double amplitude than pair (1), although they oscillate at the smae potential. From Figure (4.24), we can see that the system is synchronized almost instantly.

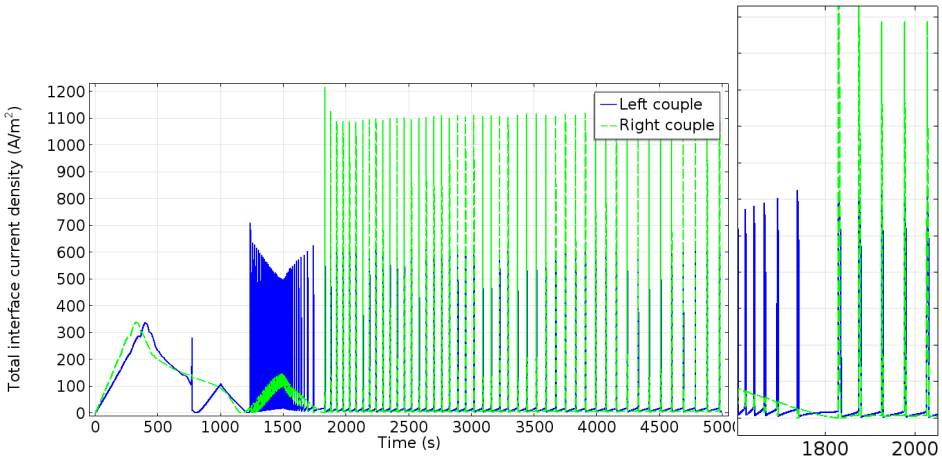

Figure 4.22: Total current densities of two anodes for the A_1C_1-A_2C_2 network.

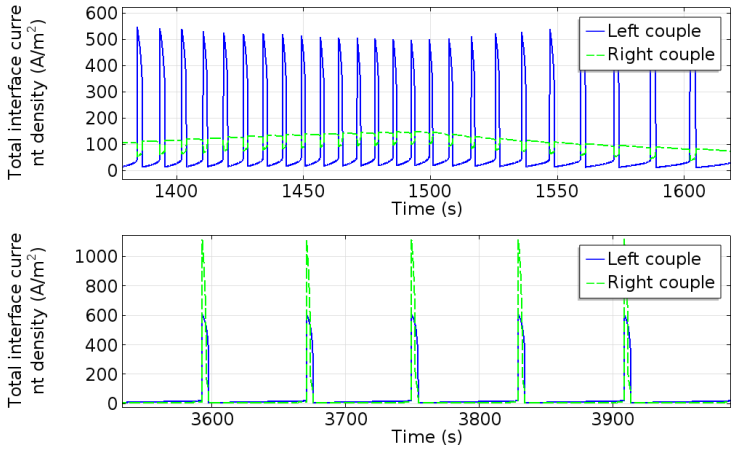

Figure 4.23: Interaction in the A_1C_1-A_2C_2 network at different time intervals.

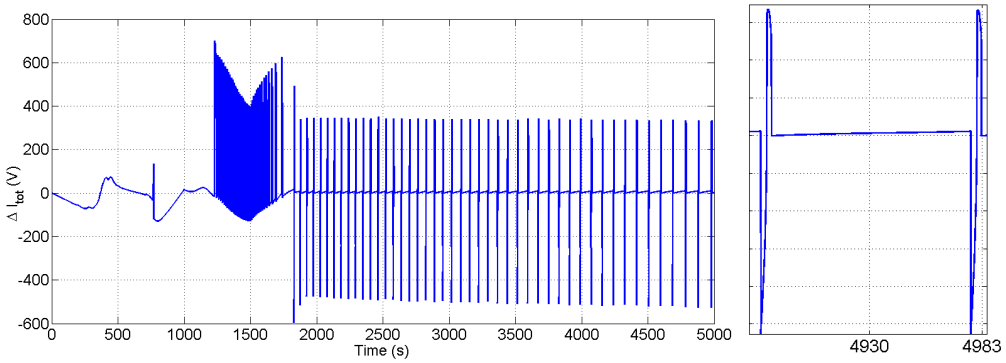

Figure 4.24: Difference of total currents of two anodes.

4.3 A_1C_1 - C_2A_2 networks

In this geometry we set the electrodes in way such that the neighbouring electrodes are the cathodes, see Figure (4.25). We start once again by calculating a cyclic voltammogram and locate the area where we interested in, see Figure (4.32). We notice that the oscillators synchronize completely. The region of the potential values where instabilities are observed is [0.7 V-0.76 V], so we chose as a high potential $\Phi_{ext} = 0.75$ V and as a low potential $\Phi_{ext} = 0.735$ V.

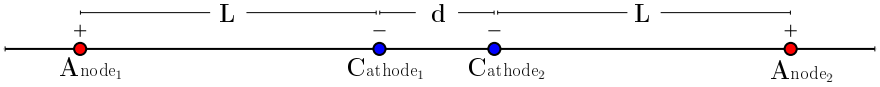

Figure 4.25: Computational domain of the A_1C_1-C_2A_2 network.

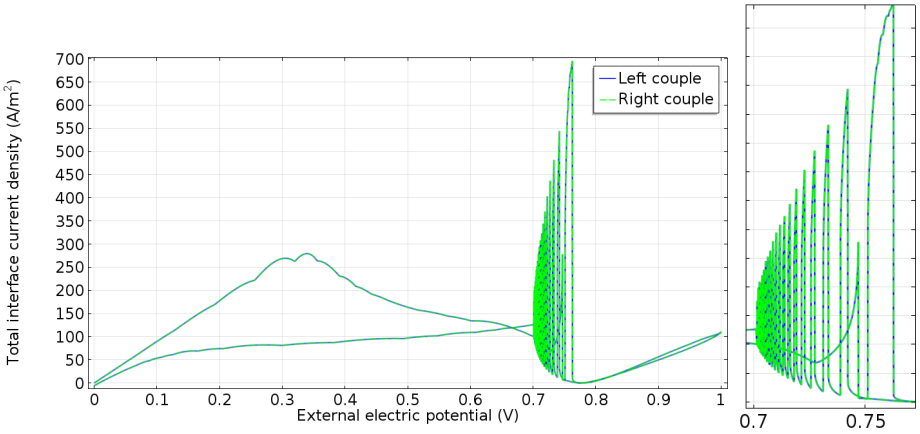

Figure 4.26: Cyclic voltammogram of the A_1C_1-C_2A_2 network .

In the next simulation we keep fixed the potential of pair (1) and compute the cyclic voltammogram of pair (2) in order to record the oscillations, Figure (4.28). Even though, both pairs are scanned with the same rate, pair (2) (green) seems to delay. While pair (1) (blue) starts to oscillate, the other pair presents damped oscillations, see Figure (4.28).

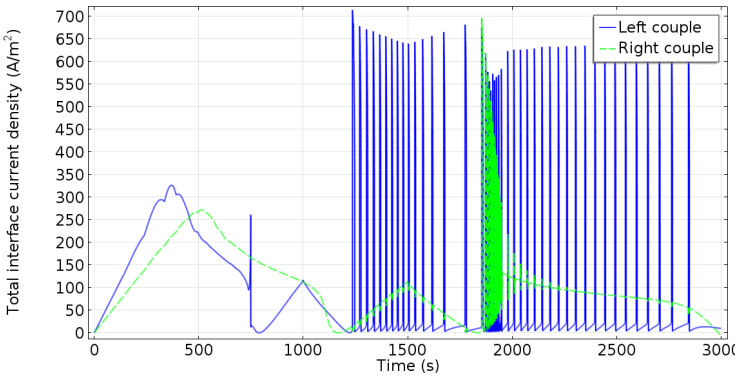

Figure 4.27: Cyclic voltammetry for pair (2) and fixed potential for pair (1) in the A_1C_1-C_2A_2 network.

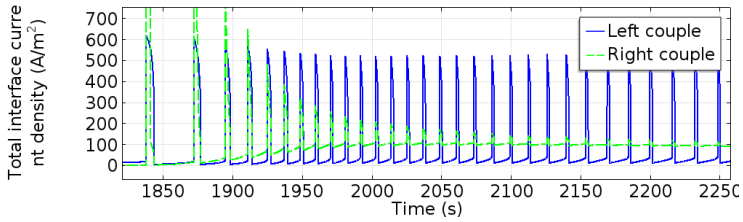

Figure 4.28: Cyclic voltammetry for pair (2) and fixed potential for pair (1) in the A_1C_1-C_2A_2 network (enlarged region).

The two oscillators are non-identical if we switch the potential form the lower value to a higher at pair (1), while pair (2) has a fixed potential value $\Phi_{\text{ext}} = 0.735$ V. We observe that synchronization is not achieved.

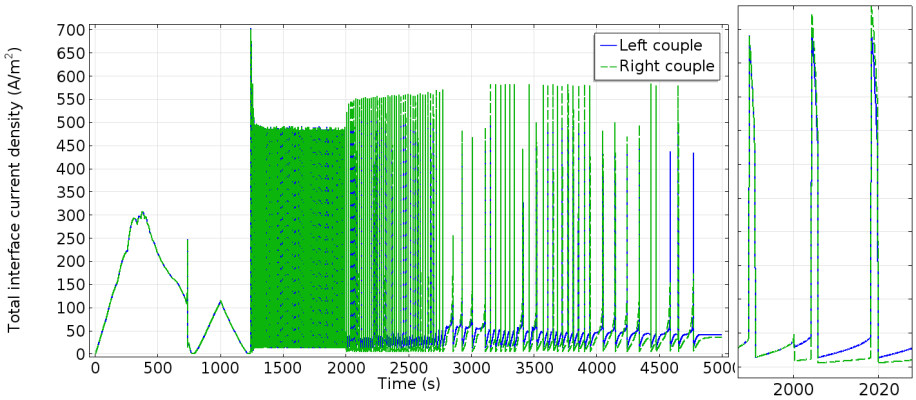

Figure 4.29: Total current densities of two anodes in the A_1C_1-C_2A_2 network.

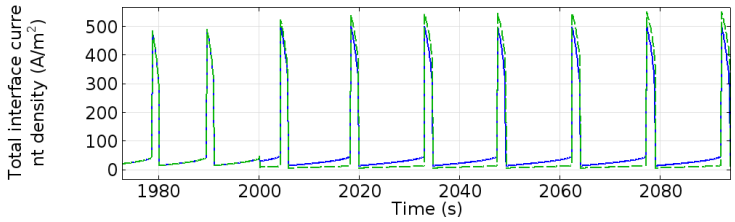

Figure 4.30: Cyclic voltammetry for pair (2) and fixed potential for pair (1) in the A_1C_1-C_2A_2 network.

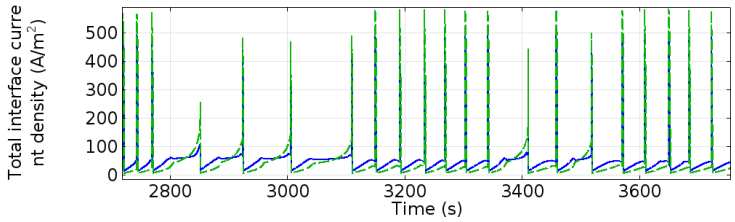

Figure 4.31: Cyclic voltammetry for pair (2) and fixed potential for pair (1) in the A_1C_1-C_2A_2 network.

By following the opposite procedure, i.e starting from higher applied potential and switching to a lower value, we see the system synchronizes and the network follows the behaviour of the oscillator being at the lower potential. The oscillations stop at 4600 s.

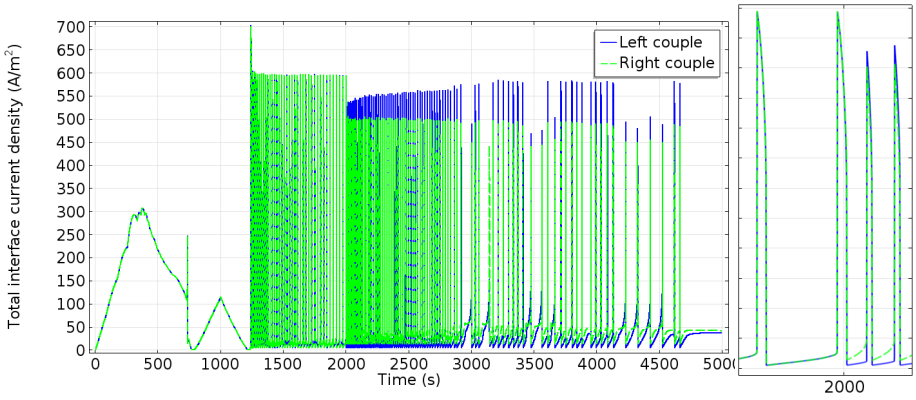

Figure 4.32: Total current densities of the two anodes.

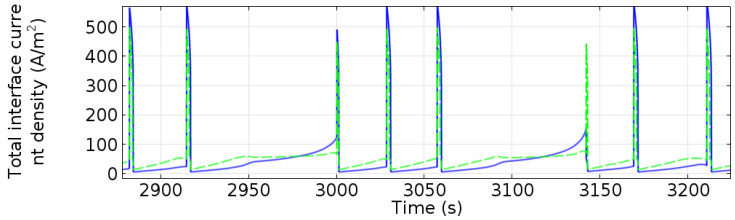

Figure 4.33: Cyclic voltammetry for pair (2) and fixed potential for pair (1).

In Figure (4.34), we apply the same value of potentials at each pair, but we scan with different rates. The pairs oscillate autonomously when both of them reach the value of 0.75 V. From the difference of total current densities, we notice that the pairs synchronize rapidly, Figure (4.35).

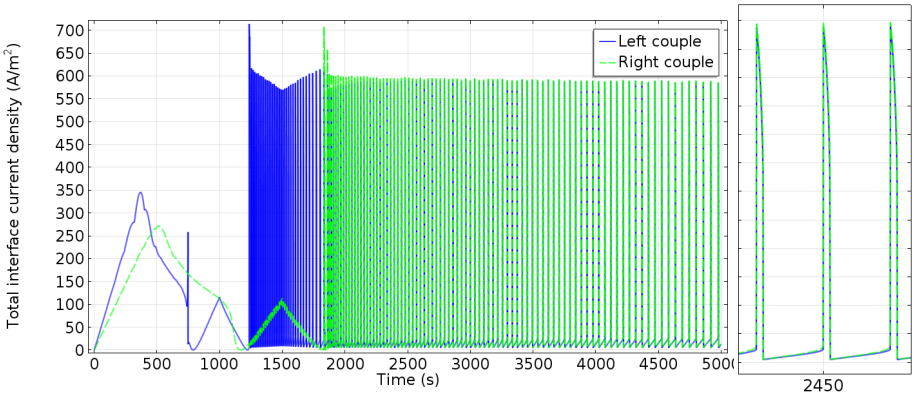

Figure 4.34: Total current densities of two anodes for $\Phi_{\text{ext}} = 0.75$ V.

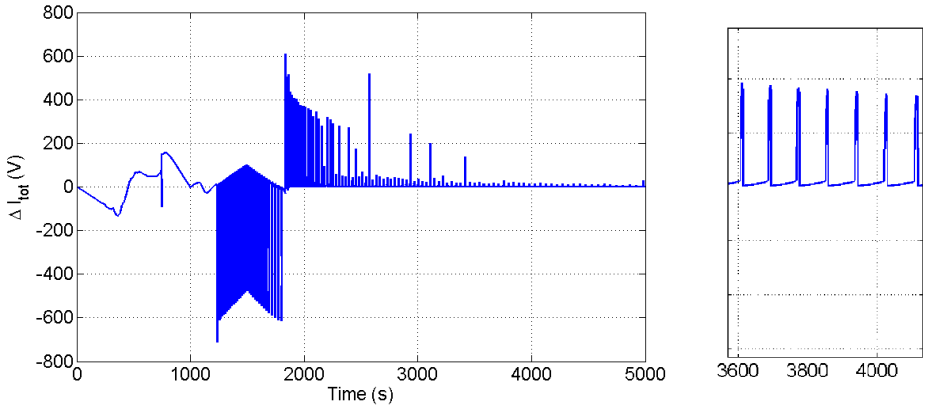

Figure 4.35: Difference of total current densities of the two anodes for $\Phi_{\text{ext}} = 0.75$ V.

Chapter 5

Conclusions

The conclusions of this work are summarized as follows:

1. Electrochemical systems following a "dissolution/passivation" mechanism exhibit instabilities leading to oscillations of the current under potentiostatic conditions. The existence of oscillations depends on the *electrochemical kinetics* and the *geometric characteristics* of the electrochemical cell.

2. Assuming *secondary current distribution* for the potential, transport of diluted species for the concentrations and the Nernst diffusion layer approximation we arrive to an ODE model which can capture the instabilities and oscillations but cannot give a realistic information for the concentration distribution.

3. The ODE formulation cannot be implemented for the modeling of realistic geometries and cannot give any information of the coupling mechanism in networks of electrochemical oscillators.

4. A *time-dependent tertiary current distribution* is the proposed model for the numerical calculation of potential and concentration distributions. This model can be solved by a finite elements scenario, implemented in COMSOL

5. In an electrochemical system consisting of an anode and a (quasi)reversible cathode, current oscillations are manifested due to the oscillations of both the electric potential and the concentrations in the solution and the electrodes surface.

6. The distribution of the potential in the solution remains, more or less, linear during oscillations. Variation of the potential is observed throughout the electrolytic cell.

7. The distribution of the concentration is constant in the "bulk" of the solution even during oscillations. The variation of the concentrations is located in a region close to the surfaces of the electrodes.

8. The potential as well as the concentration distributions *on* the electrodes are not homogeneous.

9. Networks of two oscillatory electrode pairs are able to *synchronize in-phase*. In the case of networks where the neighbouring electrodes are the anodes, synchronization is observed even if the oscillators are not identical.

10. The synchronization of oscillators is due to the flow of ionic currents between the electrodes, while they are on the "active" state of the oscillatory cycle.

11. Networks of oscillators where the neighbouring electrodes are of different nature (anode and cathode) exhibit synchrony but the amplitude of one oscillator is suppressed. The nature of coupling (inhibitory of excitatory) seems to depend on the applied potential.

12. Networks of oscillators where the neighbouring electrodes are cathodes exhibit complex oscillations. The origin of this response might be due to a competing type of coupling between the oscillatory pairs.

Bibliography

[1] G. Flätgen and K. Krischer. Accelerating fronts in an electrochemical system due to global coupling. *Phys. Rev. E*, 51(5):3997–4004, 1995.

[2] G. Flätgen and K. Krischer. A general model for pattern formation in electrode reactions. *J. Chem. Phys.*, 103(13):5428–5436, 1995.

[3] J.L. Hudson and T.T. Tsotsis. Electrochemical reaction dynamics: A review. *Chem. Eng. Sci.*, 49(10):1493–1572, 1994.

[4] A. Karantonis, L.Bieniasz, and S. Nakabayashi. The combined unidirectional and local coupling in a spatially one-dimensional model of oscillatory metal electrodissolution. patch-adaptive simulation study. *Physical Chemistry Chemical Physics*, 5(9):1831–1841, 2003.

[5] A. Karantonis, Y. Miyakita, and S. Nakabayashi. Synchronization of coupled assemblies of relaxation oscillatory electrode pairs. *Phys. Rev. E*, 65:046213, 2002.

[6] A. Karantonis, M. Pagitsas, Y. Miyakita, and S. Nakabayashi. From excitatory to inhibitory connections in networks of descrete electrochemical oscillators. *J. Phys. Chem. B*, 107:14622–14630, 2003.

[7] A. Karantonis, M. Pagitsas, Y. Miyakita, and S. Nakabayashi. In-phase, anti-phase and fractured synchrony in ring networks of coupled relaxation electrochemical oscillators. *J. Phys. Chem. B*, 108:5836–5846, 2004.

[8] I.Z. Kiss, L.N. Pelster, M. Wickramasinghe, and G.S. Yablonsky. Frequency of negative differential resistance electrochemical oscillators: theory and experiments. *Phys. Chem. Chem. Phys.*, 11:5720–5728, 2009.

[9] I.Z. Kiss, W. Wang, and J.L. Hudson. Populations of coupled electrochemical oscillators. *Chaos*, 12(1):252–263, 2002.

[10] M.T.M. Koper and J.H. Sluyters. A mathematical model for current oscillations at the active-passive transition in metal electrodissolution. *Journal of Electroanalytical Chemistry*, 347(1):31–48, 1993.

[11] K. Krischer. Spontaneous formation of spatiotemporal patterns at the electrode | electrolyte interface. *J. Electroanal. Chem.*, 501:1–21, 2001.

[12] K. Krischer. Nonlinear dynamics in electrochemical systems. In R.C. Alkire and D.M. Kolb, editors, *Advances in Electrochemical Science and Engineering*, volume 8, pages 89–208. Wiley-VCH Verlag, 2002.

[13] T. Matsuda, Y. Mukouyama, H. Hommura, S. Yae, and Y. Nakato. Identification of electrical coupling through the electrolyte as the mechanism for synchronization of electrochemical oscillations. *J. Electrochem. Soc.*, 144(9):2996–3001, 1997.

[14] Y. Miyakita, A. Karantonis, and S. Nakabayashi. Response of relaxation oscillatory electrochemical networks to external input. *Chem. Phys. Lett.*, 362:461–466, 2002.

[15] J.S. Newman. Electrochemical systems, 1991.

[16] R.D. Otterstedt, N.I. Jaeger, P.J. Plath, and J.L. Hudson. Global coupling effects on spatiotemporal patterns on a ring electrode. *Chem. Eng. Sci.*, 54:1221–1231, 1999.

[17] Ph. Russell and J. Newman. Anodic dissolution of iron in acidic sulfate electrolytes ii. mathematical model of current oscillations observed under potentiostatic conditions. *Journal of The Electrochemical Society*, 134(5):1051–1059, 1987.